DUX4-stimulated genes define the antiviral response to herpesviruses in human trophoblasts

Joshua Hatterschide[1], Liheng Yang[1], and Carolyn B. Coyne[1*]

[1]Department of Integrative Immunobiology, Duke University School of Medicine, Durham, NC, USA, Duke University Medical Center, Durham, NC, USA.

*Address correspondence:
Carolyn Coyne, PhD
3130 Medical Sciences Research Building III
3 Genome Court
Durham, NC 27710
USA
carolyn.coyne@duke.edu

Abstract

The placenta serves as a barrier against the vertical transmission of viruses, due to the protective functions of fetal-derived trophoblasts. Although some antiviral programs of trophoblasts are well-documented, our understanding of how trophoblasts respond to teratogenic viruses remains incomplete. To address this, we profiled the transcriptional responses of human trophoblast organoids to seven teratogenic viruses. We discovered that herpesviruses including HSV-1, HSV-2, and HCMV did not trigger an interferon (IFN) response but instead induced the expression of *DUX4* and downstream target genes, termed DUX4-stimulated genes (DSGs). This program was uniquely, highly expressed in trophoblasts. Through single-cell RNA sequencing, we defined the trophoblast response to *DUX4* and demonstrated that this program defines cells with low viral transcripts following HSV-1 infection. Similar to the IFN-stimulated genes, we observed that many DSGs with diverse predicted functions exhibited anti-herpesvirus activity. These findings establish DUX4 and DSGs as a critical antiviral defense mechanism in trophoblasts.

Introduction

In addition to its critical role in facilitating the exchange of nutrients, gases, and waste between the mother and fetus, the placenta acts as a robust barrier against infections, protecting the vulnerable fetus from vertical pathogen transmission during gestation.[1,2] However, certain pathogens, collectively referred to as TORCH pathogens (Toxoplasma, Other (e.g., enteroviruses, parvovirus B19, hepatitis B virus, syphilis, and Zika virus (ZIKV)), Rubella (RuV), Cytomegalovirus (HCMV), and Herpesviruses) are able to bypass the defenses at the maternal-fetal interface (MFI) and cause placental and/or fetal infections. These infections can lead to diverse pregnancy complications ranging in severity and including intrauterine growth restriction (IUGR), neurodevelopmental deficits, and loss of the pregnancy.[3-7]

The placenta is generally resistant to viral infection in part due to the antiviral activities of fetal-derived trophoblasts.[8,9] Chorionic villi of the human placenta contain several distinct subsets of trophoblasts including cytotrophoblasts (CTBs), extravillous trophoblasts (EVTs), and the syncytiotrophoblast (STB). The multinucleated STB is a single fused cell that covers the entire surface of the placenta and is in direct contact with maternal blood. CTBs are proliferative cells that lie beneath the STB and undergo fusion to grow and repair the STB layer. EVTs arise from columns of cytotrophoblasts at the tips of chorionic villi that anchor the placenta to the maternal decidua. EVTs then invade into maternal decidua (the pregnancy-specialized maternal endometrium) and remodel maternal spiral arteries to facilitate the redirection of maternal blood to the intervillous space.[10] CTBs, EVTs, and the STB are differentially susceptible to viral infection and thus may respond distinctly to pathogen infections.[2]

Responses to pathogens at the MFI must be tightly regulated as uncontrolled immune signaling at this site, such as type I interferon (IFN) signaling, is associated with poor pregnancy outcomes.[11-14] Possibly in response to this selective pressure, trophoblasts have evolved unique antimicrobial properties. For instance, the STB constitutively secretes interferon (IFN)-λs, which can act in both autocrine and paracrine manners to promote IFN-stimulated gene (ISG)

42 expression to restrict virus replication in the maternal and fetal compartments of the placenta.[9,15-
43 17] Constitutive release of IFNs is a unique feature of trophoblasts that is stimulated by viral mimicry
44 by host-derived C19MC Alu dsRNA.[16] IFN expression in most cell types is only observed after
45 the detection of pathogen associated molecular patterns (PAMPs). Evidence suggests that
46 trophoblasts also possess IFN-independent mechanisms of virus restriction. Although permissive
47 to HCMV entry, trophoblast organoids (TOs) and trophoblast stem cells have recently been shown
48 to limit HCMV replication at the stage of immediate early gene expression.[17,18] This restriction
49 occurs even in the presence of ruxolitinib, a JAK inhibitor that inhibits both type I and type III IFN
50 signaling.[17] However, IFN-independent pathways of virus restriction in trophoblasts have not yet
51 been widely explored.

52 Gaps in our knowledge surrounding how human trophoblasts respond to and defend against
53 virus infection can be attributed to the paucity of tractable systems to model the human MFI. The
54 anatomy of the MFI in many animal models is divergent from that of humans,[19,20] and animal
55 models also often require the use species-specific viruses (as in the case for HCMV)[21,22] or
56 immunodeficient or humanized animal models (as in the case of ZIKV in mice).[23] Human placental
57 explants,[24,25] isolated primary human trophoblast cells,[9] choriocarcinoma cell lines,[26] and
58 immortalized EVT cell lines[27] have all been employed to study human pathogens in their natural
59 host cells. However, these models either have a limited window of viability or lack physiological
60 properties of *in vivo* trophoblasts.[28] Trophoblast organoids are an *in vitro* model of the placenta
61 that is able to overcome some of the limitations of previous models. TOs and matched maternal
62 decidua organoids (DOs) can be derived from chorionic villi at early and late stages of
63 gestation.[17,29,30] TOs spontaneously differentiate into EVTs and the STB and constitutively secrete
64 hormones such as human chorionic gonadotropin (hCG) and immune molecules such as IFN-λs
65 that are naturally secreted by trophoblasts *in vivo*.[17]

66 In this study, we profiled the transcriptional responses of TOs to seven teratogenic viruses to
67 define cell-intrinsic mechanisms of virus restriction in trophoblasts and to determine whether they

68 responded in a virus-specific manner. We found that TOs mounted distinct responses to RNA and
69 DNA viruses, with the transcription factor DUX4 dominating the response to herpesviruses. DUX4
70 is a primate-specific pioneering transcription factor that participates in zygotic genome activation[31]
71 and is typically restricted to the 4-8 cells stages of embryonic development. Aberrant expression
72 of DUX4 in adult somatic muscle cells is the cause of facioscapulohumeral muscular dystrophy
73 (FSHD).[32,33] Expression of DUX4 has been observed following herpesvirus infection in other
74 systems and select DUX4-stimulated genes (DSGs) were previously reported to restrict
75 herpesvirus replication.[34,35] Comparative transcriptional profiling in TOs and DOs derived from
76 matched donor tissue infected with HCMV and HSV-1 revealed that the DUX4 program is
77 enriched in TOs, which occurs independent of constitutive type III IFN signaling. Using single cell
78 RNA sequencing (scRNAseq), we characterized the DUX4 program in trophoblasts in the context
79 of both an inducible DUX4 expression system and HSV-1 infection. DUX4 and accompanying
80 DSGs were observed to define a low viral gene expression trajectory in HSV-1 infected TOs. To
81 define the antiviral activity of DSGs, we performed high-content screening of the 30 top-most
82 induced DSGs in TOs for antiviral activity against herpesviruses in naturally permissive cells.
83 Analogous to ISGs in the IFN pathway, we observed redundancy in the antiviral activity of DSGs.
84 This shifts our understanding of DUX4 and DSGs from a collection of isolated antiviral genes to
85 a concerted antiviral signaling program that retains key hallmarks of ISGs, including a robust and
86 overlapping antiviral gene induction mechanism. Together, these findings unveil a human
87 trophoblast-enriched anti-herpesvirus pathway that mirrors the functional principles of the IFN
88 response, providing new insights into host defense strategies against viral infections at the
89 maternal-fetal interface.

Results

Human trophoblast organoids respond distinctly to diverse viruses

To directly compare how human placental trophoblasts respond to infection with teratogenic viruses, TOs from two male donors (TO74 and TO90) and one female donor (TO81) were infected with seven teratogenic viruses that belong to diverse virus families. These viruses included three herpesviruses: HCMV, HSV-1, HSV-2, a poxvirus: Vaccinia virus (VACV), and three positive sense RNA viruses: echovirus 5 (Echo5), rubella virus (RuV), and Zika virus (ZIKV). RNA was collected from mock and infected TOs and sent for polyA-selection bulk RNA sequencing. Reads were mapped to both the human and viral genomes. We observed minimal mapping of reads to the viral genomes in mock samples and little donor-to-donor variation in viral read levels in infected samples **(Figure S1A)**. Reads mapping to the virus genomes were excluded for the remaining analyses.

Differential gene expression analysis was conducted using the DESeq2 package, incorporating donor as a factor in the statistical model to account for variability between individual donors.[36] Differentially expressed genes (DEGs) were defined as host genes with Log_2 (fold-change) > 1 and adjusted *p*-value < 0.05. The differences in magnitude of the induced responses ranged from zero DEGs following ZIKV infection to 5453 DEGs following VACV infection **(Figure 1A-G and Table S1)**. We also observed variability in the directionality of responses. HSV-1, HSV-2, and RuV all led to substantially more upregulated DEGs than downregulated. HCMV and VACV both led to a relatively even distribution between upregulated and downregulated DEGs. Echo5 was the only virus with a response that skewed toward downregulation **(Figure 1A-G)**. The small transcriptional responses elicited by Echo5 and ZIKV may arise from impaired virus replication in TOs, which would lead to lower levels of pathogen associated molecular pattern (PAMP) detection and a diminished transcriptional response. This is consistent with what we've shown for ZIKV previously,[17] and with the observation that these viruses had the lowest quantities of viral reads **(Figure S1A)**. Pairwise comparisons between each infection condition revealed some overlap in

upregulated and downregulated DEGs between these diverse viruses **(Figure 1H).** However, after excluding Echo5 and ZIKV (due to their limited responses), only two DEGs were upregulated by all of the five remaining viruses: *EGR3* and *THBS1*. This suggests that TOs respond distinctly to infection in a virus-specific manner.

To further categorize these responses, we performed a principal component analysis (PCA). Four groups were found to segregate from the mock-infected samples along the first four principle components: HSV-1- and HSV-2-infected, VACV-infected, RuV-infected, and HCMV-infected **(Figure 1I)**. As expected, Echo5- and ZIKV-infected samples clustered closely with the mock-infected samples. We next analyzed the loadings from the PCA to identify sets of genes that defined these unique responses. The response to VACV was predominantly defined by genes encoding histone variants such as *H3C1* and *H4C2* **(Figure 1J, middle left)**. RuV was the only virus that induced type-I and type-III interferon (IFN) genes such as *IFNB1* and *IFNL1* along with downstream interferon-stimulated genes (ISGs) including *OASL*, *IFIT2,* and many others **(Figure 1J, middle right)**. The unique response to HCMV was defined by genes such as *IVL*, *IL1RN*, and *MPZL2* **(Figure 1J, right)**. HSV-1- and HSV-2- infected samples were defined by tripartite motif family genes such as *TRIM43* and *TRIM49*, and preferentially expressed antigen of melanoma family genes such as *PRAMEF8* and *PRAMEF12* **(Figure 1J, left)**.

Many of the genes that defined the HSV-1- and HSV-2- infected samples were also induced by HCMV. Indeed, there were 28 genes induced by all three herpesviruses **(Figure S1B)**. Most of these shared DEGs were induced by the herpesviruses and no other viruses **(Figure S1C)**. These findings suggest the existence of a herpesvirus-specific pathway activated in trophoblasts.

Trophoblasts respond to herpesviruses with DUX4-stimulated genes

Several of the shared differentially expressed genes induced by HSV-1, HSV-2 and HCMV, such as *TRIM43*, are putative targets of the transcription factor DUX4. DUX4 is a pioneering transcription factor that is normally expressed during embryogenesis between the four-cell and

142 eight-cell stages[31] and is pathogenic when aberrantly expressed in adult muscle cells.[32,33] DUX4
143 has also been shown to be upregulated following HSV-1 infection.[34] In the TO infection bulk
144 RNAseq analyses, *DUX4* expression was up-regulated in all donors by HSV-1 and HSV-2 and by
145 two donors by HCMV **(Figure 2A)**. DUX4 was not detected in any other infection conditions.
146 However, *DUX4* expression is notoriously difficult to detect even using next generation
147 sequencing methods.[37,38] Therefore, we confirmed the expression of *DUX4* and the DUX4
148 transcriptional-target, *TRIM43*, only in herpesvirus-infected samples in all three donors using
149 qRT-PCR **(Figure S2A-B)**.

150 DUX4 has never been studied in trophoblasts, and DUX4-stimulated genes (DSGs) in these
151 cells have yet to be defined. To characterize DSGs in trophoblasts, we developed a model of
152 DUX4 expression in TOs. TOs from three donors were transduced with a lentiviral vector encoding
153 codon-optimized DUX4 under a doxycycline-inducible promoter (iDUX4). Transduced organoids
154 were selected with puromycin, and expression of DUX4 upon treatment with doxycycline was
155 confirmed by immunofluorescence **(Figure 2B)**. One strength of the TO model is that they retain
156 the capacity to differentiated into several lineages of trophoblasts present in the placenta *in vivo*.
157 To define DSGs across trophoblast cell types, and to determine whether there were trophoblast
158 cell type-specific DSGs, doxycycline-treated and mock-treated organoids from three donors were
159 dissociated and analyzed by single-cell (sc)-RNAseq. A total of 23,981 doxycycline-treated cells
160 and 23,233 mock-treated cells passed quality control and were used for further transcriptional
161 analysis following integration to correct for donor and batch effects. Clustering analysis revealed
162 11 clusters of cells that were present in both conditions **(Figure 2C and Figure S2C)**. The
163 identities of the clusters were defined by the expression of canonical trophoblast marker genes[39-
164 41] **(Figure S2E-F)**. The proliferative CTB clusters (CTBp-1, -2, and -3) were defined by high
165 expression of *MKI67*, *CCNA2*, *PCNA*, and *TOP2A*. CTB clusters (CTB-1, -2, -3, and -4) were
166 defined by cells that express high levels of the pan-trophoblast markers *PAGE4*, *PEG10*, *SMAGP*,
167 and *TP63*, but lack expression of more specialized programs. Of note, CTBp-1 and CTB-4 also

168 expressed markers of cell column CTBs such as *ITGB6*, *ATF3*, *PLAC8*, and *PLAU*. Cells in the
169 process of fusing into the STB (STBpre) were defined by the expression of the endogenous
170 retroviral elements that mediate and modulate fusion such as *ERVV-1*, *ERVFRD-1*, *ERVW-1*, and
171 *ERVE-1*. Markers of STB function including *HOPX*, *SDC1*, *CGB5*, and *PSG3* were used to define
172 the STB cluster. Two clusters were classified based on high iDUX4 expression in the doxycycline-
173 treated samples (DUX4-high-1 and DUX4-high-2). The presence of some cells in the "DUX4-high"
174 clusters in the mock-treated sample is likely due to leaky expression of iDUX4. The DUX4-high-1
175 cluster expands from an average of 1.6% of the mock-treated cells to an average of 11.6% of the
176 doxycycline-treated cells **(Figure S2D)**. The remaining clusters occupied a similar proportion of
177 cells between donors and conditions.

178 We first sought to identify genes that were broadly controlled by DUX4 across cells in the
179 dataset. We calculated the Pearson's correlation coefficient (r) between the expression of iDUX4
180 and other genes across all cells. One hundred and fifty genes were found to positively correlate
181 with iDUX4 expression with $r > 0.4$ suggesting they are stimulated by iDUX4 and can be classified
182 as DSGs **(Figure 2D and Table S2)**. To test whether these genes were similar to DSGs in other
183 cell types, we generated a list of 101 cell-type-independent DSGs (DUX4.101) by reanalyzing and
184 comparing bulk RNAseq datasets in which DUX4 was overexpressed in iPSCs (a model of DUX4
185 in embryogenesis)[31] and MB135 cells (a model of DUX4 in muscular dystrophy)[42] **(Figure S3A-C
186 and Table S3)**. The expression of many of the genes in the DUX4.101 list strongly correlated with
187 iDUX4, suggesting the DUX4 program in TOs is similar to that of other cell types **(Figure 2D)**. We
188 also confirmed overlap between the DUX4.101 list and genes controlled by DUX4 in TOs by
189 performing bulk RNAseq on doxycycline-treated and mock-treated organoids **(Figure S3D-E and
190 Table S3)**. While there were many genes uniquely modulated by iDUX4 in TOs, these data
191 demonstrate that the canonical DUX4 program is induced in trophoblasts. 98 of the genes that
192 correlated with iDUX4 expression with $r > 0.4$ were not a part of the iDUX4 list, including *GTF2F1*,
193 *PTP4A1*, *DBR1*, *ODC1*, *SOX15* amongst others.

194 We next investigated which trophoblast cell types predominantly expressed the DUX4 pathway
195 and whether it could be activated in a trophoblast cell type-specific manner. Expression of genes
196 in the DUX4.101 list were elevated in the doxycycline-treated samples and predominantly found
197 in the two DUX4-high clusters **(Figure 2E-F)**. This demonstrates that cells that express iDUX4
198 are transcriptionally distinct enough to cluster separately from other trophoblasts. As iDUX4
199 expression could also be observed in the non-DUX4-high clusters **(Figure 2F)**, we next defined
200 the impact of iDUX4 expression in these cell types. We performed pseudobulk analysis to identify
201 DEGs between the doxycycline-treated and mock-treated samples for each cluster. Although
202 there were cluster-specific differences in DEGs, genes in the DUX4.101 list were found to be
203 among the most highly differentially expressed genes across all clusters **(Figure 2G and Table**
204 **S4)**. These data demonstrate that many of the canonical DSGs are also induced by DUX4
205 expression in trophoblasts and that DUX4 expression is capable of driving the expression of these
206 genes in all trophoblast lineages.

207 Finally, we determined whether any of the DEGs induced in TOs in response to herpesvirus
208 infections were DSGs. We found that the DUX4.101 list significantly overlapped with the top 100
209 DEGs induced by HCMV, HSV-1, and HSV-2, while overlapping by only one gene each with the
210 top DEGs induced by VACV and RuV **(Figure 2H and Figure S3F-K)**. HCMV may have induced
211 fewer DSGs than HSV-1 or HSV-2 due to its impaired replication in trophoblasts [17,18]. Based on
212 these data, we conclude that many of the shared genes induced by herpesviruses in TOs are
213 DSGs.

214

215 **DUX4-stimulated genes are induced to higher levels in trophoblasts organoids than**
216 **maternal-derived decidua epithelial organoids**

217 TOs repress HCMV replication and differentially respond to HCMV when compared to maternal
218 decidua derived DOs.[17,18] Because DSGs were upregulated in response to herpesviruses in TOs,
219 we determined whether this pathway was differentially induced in TOs and DOs following

220 herpesvirus infection. Matched TOs and DOs were mock-treated or infected with HSV-1 (MOI of
221 5). RNA was collected and sent for polyA selection bulk RNA sequencing. Additionally, we
222 reanalyzed published RNA sequencing data from the infection of TOs and DOs with the HCMV
223 strains TB40/E and AD169r (a clone of AD169 engineered to express the HCMV pentameric
224 complex).[43] All RNA sequencing datasets were remapped to the human transcriptome following
225 the same pipeline and analyzed using DESeq2 **(Table S5)**. We found that DUX4 expression was
226 more than 9-fold higher in TOs than DOs following infection with HCMV TB40/E **(Figure 3A)**,
227 HCMV AD169r **(Figure 3B)**, and HSV-1 **(Figure 3C)**. Analysis of the top 100 upregulated DEGs
228 following each infection revealed greater overlap between the DEGs of TOs and the DUX4.101
229 list compared to the DEGs of DOs **(Figure 3D)**. While these DSGs were highly induced in TOs,
230 nearly all of them were not induced in DOs following infection with HCMV TB40/E or HCMV
231 AD169r **(Figure 3E and Figure S4A-D)**. Although DSGs were induced following HSV-1 infection
232 in both TOs and DOs, all were induced between 6- and 50-fold more in TOs **(Figure 3E and**
233 **Figure S4E-F)**. We used qRT-PCR to confirm enhanced expression of *DUX4* and the DSGs
234 *TRIM43B* and *PRAMEF1* in three donors of TOs compared to three donors of DOs following
235 HCMV TB40/E infection **(Figure S4G-I)**. These data demonstrate that trophoblasts respond with
236 higher expression of *DUX4* and DSGs than maternal decidua epithelial cells.
237

238 **Expression of DUX4 and DSGs is not dependent on constitutive type-III IFN signaling**

239 The mechanisms by which DUX4 and DSG expression are induced by herpesviruses remain
240 unknown. Additionally, the signaling pathways that modulate this program to drive its heightened
241 expression in TOs have yet to be identified. Trophoblasts constitutively secrete type III IFNs,
242 which is a major innate immunological difference between TOs and DOs.[17] Although DUX4 and
243 DSG expression has not been previously linked to type-III IFN signaling, it could explain the
244 increased expression of DUX4 and DSGs in TOs over DOs. To test this, we generated *IFNLR1*
245 knockout (KO) TOs using CRISPR-Cas9 and a single guide RNA (sgRNA) targeting exon three

246 of the *IRNLR1* locus. To validate KO of *IFNLR1* genetically, we amplified the sgRNA target site
247 using high-fidelity PCR and sequenced the product using Sanger sequencing. Using the ICE tool
248 (Synthego) to predict the mixture of insertions and deletions present in the mixture, we found -19
249 bp and -10 bp deletions >95% of the sequences in the IFNLR1 KO clone **(Figure 4A-B)**. To test
250 whether IFNLR1 KO TOs are responsive to type-III IFNs, parental and IFNLR1 KO organoids
251 were treated with recombinant IFNλ3. RNA was collected and qRT-PCR was used to measure
252 the expression of several ISGs. Whereas *OASL* and *MX1* were induced ~ 5-fold and 10-fold
253 respectively in the parental TOs treated with IFNλ3, neither was induced in IFNLR1 KO TOs
254 **(Figure 4C-D)**. Additionally, *OASL* and *MX1* were expressed at a significantly lower baseline-
255 level in IFNLR1 KO cells, likely due to disruption of constitutive autocrine type III IFN signaling.
256 IFNLR1 KO and parental cells were infected with HSV-1 to induce the expression of DUX4 and
257 DSGs. RNA was collected from mock and infected organoids and qRT-PCR was used to measure
258 the expression of the HSV-1 immediate early transcript ICP4, *DUX4*, and the DSGs: *TRIM43* and
259 *PRAMEF1*. HSV-1 ICP4 was expressed at similar levels in parental and IFNLR1 KO cells,
260 suggesting that type III IFN signaling does not restrict HSV-1 replication **(Figure 4E)**. *DUX4*
261 expression was increased in IFNLR1 KO TOs and *TRIM43* and *PRAMEF1* were expressed at
262 similar levels in control and KO organoids **(Figure F-H)**. These data suggest that the increased
263 expression of *DUX4* and DSGs in TOs occurs through a mechanism independent of type-III IFN
264 signaling.
265

266 **DUX4-stimulated genes define a low viral gene expression trajectory in HSV-1-infected**
267 **trophoblast organoids**

268 To further define the relationship between the DUX4-DSG program and herpesvirus infections
269 in trophoblasts, we next investigated which trophoblast cell types express this program in
270 response to infection and examined how the expression of these genes compared to that of viral
271 genes. HSV-1-infected and mock-infected organoids from two donors (2x TO74 samples and 1x

272 TO84 sample each) were dissociated and analyzed by scRNAseq. A total of 14,846 HSV-1-
273 infected cells and 13,881 mock-infected cells passed quality control and were used for further
274 analysis following integration to correct for donor and batch effects. Clustering analysis revealed
275 11 clusters of cells that were present in both conditions **(Figure 5A and Figure S5A-C)**. The
276 identities of the clusters were defined by the expression of the canonical trophoblast marker genes
277 described above[39-41] **(Figure S5D-J)**.

278 We first investigated which cells expressed DUX4/DSG and HSV-1 transcripts. We found that
279 *DUX4* and DSGs were only expressed in HSV-1-infected samples, with one CTB cluster exhibiting
280 particularly high levels of their expression (termed "DUX4-high"). *DUX4* and DSG expression was
281 also high in the STB cluster **(Figure 5B and Figure S5I)**. In contrast, most HSV-1 transcripts,
282 including all transcripts classified as late genes (γ1 and γ2) were expressed highest in a distinct
283 CTB cluster (termed "HSV-1-high") **(Figure 5C and Figure S5J-K)**. A handful of immediate early
284 (α), early (β), and unclassified HSV-1 genes were expressed at comparable or higher levels in
285 the DUX4-high cluster when compared to the HSV-1-high cluster. As HSV-1 genes expression
286 could be observed outside of the HSV-1- and DUX4-high clusters **(Figure 5B-C)**, we next
287 investigated how HSV-1 infection impacted gene expression in those clusters. We performed
288 pseudobulk analysis to determine differential gene expression between the HSV-1-infected and
289 mock-infected samples in each of these clusters **(Figure 5D and Table S6)**. Other than HSV-1
290 genes, DSGs were found to be among the most highly DEGs in all clusters. These data
291 demonstrate that all trophoblast lineages in TOs can respond to HSV-1 infection with the
292 expression of DUX4 and DSGs.

293 The observation that peak DUX4/DSG expression and peak HSV-1 transcript expression were
294 found in separate HSV-1-infected clusters suggests two possibilities: 1) that DUX4 and DSG
295 expression precedes maximal HSV-1 gene expression during the normal course of replication, or
296 2) that DUX4 and DSG expression defines a distinct fate of HSV-1-infected cells in which
297 replication is impaired. To determine which was the case, we performed trajectory analysis which

298 seeks to computationally infer the ordered progression of cells along a “pseudotime.” Cells from
299 HSV-1-infected samples with > 0.1% of reads mapping to the HSV-1 genome were re-analyzed
300 independently **(Figure 5E)**. Clustering yielded eight clusters that were defined as described for
301 previous analyzes **(Figure S6A-I)**. Trajectories were predicted using the Slingshot algorithm
302 starting with the CTB-2 cluster and with undefined end clusters.[44] Three trajectories were inferred,
303 one that leads toward peak DSG expression (pseudotime 1), one that leads toward the peak of
304 HSV-1 gene expression (pseudotime 2), and one that follows differentiation into the STB
305 (pseudotime 3) **(Figure 5F)**. We performed pseudobulk analysis comparing cells at the termini of
306 pseudotime 1 and 2 to determine differential gene expression. We found that all but one HSV-1
307 transcript was more highly expressed in terminus 2 than 1 **(Figure 5G)**. Conversely, 64 DSGs
308 from the DUX4.101 list were more highly expressed in terminus 1 than 2. Four DSGs followed the
309 opposite pattern, and the remainder were not statistically significant. To visualize gene expression
310 patterns along these trajectories, fitGAM was used to calculate the average expression of HSV-1
311 transcripts and DSGs along pseudotime trajectories 1 and 2. While HSV-1 transcripts increased
312 along pseudotime 1, most reached only a small fraction of peak expression **(Figure 5H)**. All but
313 two HSV-1 transcripts instead reached maximum gene expression along pseudotime 2. DSGs
314 followed the opposite pattern. Nearly all DSGs reached peak expression along pseudotime 1,
315 while they reached only a fraction of peak expression along pseudotime 2 **(Figure 5I)**.
316 Interestingly, peak DSG expression comes after the rise and fall of HSV-1 genes expression along
317 pseudotime 1. This pattern is borne out by the expression of representative features such as the
318 percent of transcripts mapping to HSV-1, GFP expression from the HSV-1 genome, and
319 expression of DSGs *TRIM49* and *PRAMEF1* **(Figure 5J-K and Figure S6H-I)**. Taken together,
320 these data suggest that high DSG expression defines a low viral gene expression trajectory in
321 HSV-1-infected trophoblasts.
322
323 **DUX4-stimulated genes exert anti-herpesvirus activity**

324 Given that DUX4 and DSGs are highly upregulated in response to herpesviruses and define a
325 trajectory associated with low viral gene expression following infection, we next sought to test
326 whether these genes exhibited anti-herpesvirus activity. As the cause of FSHD, many studies
327 have attempted to engineer cells to block or impair DUX4 expression[45]. In genetically normal cells,
328 hundreds of copies DUX4 coding sequence are repeated within D4Z4 arrays that are located in
329 the proximal sub-telomeric domains of chromosomes 4 and 10. D4Z4 has additional homologous
330 regions in many other chromosomes.[46] For this reason, traditional CRIPSR-Cas9 editing within
331 the DUX4 ORF is not generally employed as it would generate many double-stranded breaks,
332 leading to genome instability and off-target effects.[45] Instead, studies have employed CRISPR
333 interference (CRISPRi),[47] CRISPR/Cas9-directed base editing,[48] and dominant-negative DUX4
334 constructs,[49] all with varying degrees of knockdown efficiency. We attempted several similar
335 methods of impairing DUX4 activity in TOs including *DUX4*-targeting shRNAs **(Figure S7A-D)**,
336 CRISPRi targeting the transcription start site of the *DUX4* locus **(Figure S7E-G)**, and a dominant-
337 negative DUX4 construct where the transactivation domain was swapped for the KRAB domain
338 of ZIM3 **(Figure S7H-L)**. Although we achieved modest suppression of *DUX4* using shRNAs and
339 of the DSGs *TRIM43* and *PRAMEF1* using the DUX4-ZIM3 construct, DSGs in these contexts
340 were still expressed at ~250- and 500-fold more than in mock samples (which were at or near the
341 limit of detection). Accordingly, these interventions had insignificant impact on HSV-1 gene
342 expression **(Figure S7D and L)**. For this reason, we decided to instead interrogate the top DSGs
343 induced by herpesviruses in TOs for anti-herpesvirus activity.

344 The biological functions of DSGs are largely unknown. Therefore, we systematically screened
345 individual DSGs for antiviral activity against HCMV and HSV-1 using an overexpression system
346 in cells permissive to virus replication. We selected DSGs that were highly induced in response
347 to iDUX4 expression, and HCMV TB40/E, HCMV AD169r, or HSV-1 infection **(Figure S8A)**. Many
348 DSGs were within transposable elements, causing them to have many orthologues in the human
349 genome which are often other DSGs.[31] Among DSGs with >90% peptide identity, a single ORF

350 was selected **(Figure S8B)**. The remaining genes were prioritized to a list of 30 based on median
351 log_2 (fold-change) in TO datasets **(Figure S8C)**. Codon-optimized ORFs of these genes were
352 cloned into lentiviral expression vectors that co-expressed puromycin resistance and Tag2BFP
353 on a polycistronic transcript **(Figure 6A)**. MRC5 cells, which are permissive to HCMV and HSV-
354 1, were arrayed in 96-well plates and transduced with these lentiviruses as well as a control
355 lentivirus (ORF_Stuffer) and a vector expressing a codon-optimized *DUX4* ORF. Cells were
356 selected with 2 µg/mL puromycin for 48 h. Cells were then infected with 5 x 10^4 pfu / well of HCMV
357 TB40/E (mCherry) or 5 x 10^3 pfu / well of HSV-1 (GFP-UL25). These infection conditions were
358 chosen to observe a single round of HCMV replication in a high percentage of cells over 96 h,
359 while allowing for multiple rounds of HSV-1 replication over a similar timespan. Replication
360 progression was monitored over time using high-content automated fluorescence microscopy
361 **(Figure 6A)**. Overexpression of six DSGs as well as DUX4 exhibited cell toxicity in MRC5 cells
362 **(Figure S8D-E)**.

363 Fluorescence intensity of the exogenously expressed tags was quantified, and hits at each
364 timepoint were defined as conditions that reduced the fluorescence intensity to less than half of
365 that of ORF_Stuffer **(Figure S8F)**. We observed 17, 21, 18, and 15 hits for HCMV at 1, 2, 3, and
366 4 dpi respectively **(Figure 6B and Figure S9A-C)**. 13, 10, and 8 hits were observed for HSV-1 at
367 1, 2, and 3 dpi **(Figure 6C and Figure S9D-E)**. Ten genes consistently restricted replication of
368 both viruses: *CCNA1*, *FRG2*, *H3Y1*, *LEUTX*, *MBD3L2*, *PRAMEF2*, *PRAMEF8*, *PRAMEF20*,
369 *PRR20D*, and *TRIM49* **(Figure 6D-E)**. A handful of candidates were found to be antiviral to HCMV
370 but not HSV-1. These included *PRAMFE12* and *ZSCAN4*, both of which consistently reduced
371 mCherry expression from HCMV to less than 25% of ORF_Stuffer while having minimal impact
372 on GFP expression from HSV-1 **(Figure 6E)**. The top hits from both viruses suppressed
373 fluorescence protein expression throughout all timepoints **(Figure 6F-I)**. These data show that
374 many DSGs function as antiviral mediators.

375 ## Discussion

376 Fetal-derived trophoblasts form the barrier between the maternal and fetal compartments of
377 the MFI and possess cell-autonomous mechanisms of protecting the developing fetus from the
378 vertical transmission of viruses.[1,2] Furthermore, trophoblasts have been shown to restrict the
379 replication of prominent teratogenic herpesviruses such as HCMV.[17,18] In this study, we profiled
380 the response of TOs to seven teratogenic viruses and identified the expression of DUX4 and
381 downstream target DSGs as a unique response to herpesvirus infections. Comparison between
382 TOs and matched maternally-derived DOs revealed that DUX4 and DSGs are induced to
383 significantly higher levels in TOs by both HSV-1 and HCMV, suggesting that it is uniquely induced
384 in trophoblasts. Using scRNAseq and pseudotime trajectory analysis, we identified a unique
385 pathway in HSV-1-infected TOs. This trajectory was distinct from the typical virus replication
386 trajectory and was characterized by the expression of *DUX4* and downstream target DSGs.
387 Overexpression of the most highly induced DSGs in cells permissive to HSV-1 and HCMV
388 replication demonstrated that many of these genes significantly impaired the replication of one or
389 both viruses. These findings uncover a previously unrecognized antiviral pathway in human
390 trophoblasts, wherein the induction of DUX4 and its downstream target genes serves as a cell-
391 intrinsic defense mechanism against herpesvirus infections. This discovery highlights the unique
392 antiviral strategies employed by trophoblasts to protect the developing fetus from teratogenic viral
393 threats.

394 A relationship between the DUX4 program and herpesvirus infection has emerged, but there
395 is not a consensus on its role in virus replication. Expression of DUX4 or select DSGs have been
396 observed in response to infection with alpha, beta, and gamma herpesviruses in cell culture as
397 well as in herpesvirus-mediated cancers.[34,50-52] Induction of DUX4 following herpesvirus infection
398 was originally described based on the antiviral activity of the E3 ubiquitin ligase TRIM43.[34]
399 TRIM43 was proposed to impair herpesvirus replication by directing components of the
400 centrosome for degradation leading to destabilization of the nuclear envelope.[34] Recently,

401 knockdown of the DSGs *RASD1* and *RRAD*, which are Ras-related GTPases, was found to
402 augment HSV-1 virion production in fibroblasts.[35] As the above DSGs exert antiviral activity,
403 DUX4 and DSGs have been suggested to be a part of the cell-intrinsic defenses against
404 herpesvirus infection. In the cell types examined in previous studies, DSG induction typically
405 occurs alongside canonical IFN antiviral signaling, which likely serves as the primary antiviral
406 defense mechanism. In contrast, our findings reveal that in human trophoblasts, the DUX4
407 pathway operates as the predominant defense mechanism against herpesvirus infections,
408 representing a specialized antiviral strategy unique to this cell type. Consistent with this, we found
409 that the expression of DUX4 and the majority of DSGs defined a low viral gene expression
410 trajectory following HSV-1 infection in TOs. In line with this, overexpression of the majority of
411 DSGs restricted HSV-1 and/or HCMV replication in MRC5 fibroblasts. Our data expands our
412 conception of DUX4 and DSGs from isolated antiviral genes controlled by a common transcription
413 factor to a coordinated cell-intrinsic antiviral pathway.

414 Most DSGs are not expressed at detectable levels in normal adult cells, and many remain
415 largely uncharacterized. Their specific roles and potential functions are poorly understood,
416 highlighting a significant gap in our knowledge about these genes and their biological importance.
417 Apart from *TRIM43*, *RASD1*, and *RRAD*,[34,35] it remained unclear how many DSGs exert anti-viral
418 activity. Thus, we tested the impact of overexpression of 30 DSGs that were highly expressed in
419 TOs on HSV-1 and HCMV replication in permissive MRC5 cells. Twenty-one of these genes
420 reduced fluorescent protein expression of at least one virus by >50% during at least one timepoint.
421 If we extrapolate to include genes that were excluded based on the >90% peptide identity cutoff,
422 this screen identified 42 novel potentially antiviral human ORFs. Of note, one of the three genes
423 that had little impact on the replication of either virus at any timepoint was *TRIM43*. *RASD1* and
424 *RRAD* were not tested in this screen because they did not meet the expression cutoffs in TOs for
425 inclusion. Additionally, none of the DSGs in the screen led to an increase in viral fluorescent
426 protein expression above that of the control vector. One of the top antiviral DSGs identified by the

427 screen was *CCNA1*, which is a meiosis-specific cyclin A gene in mammals.[53] Although, *CCNA1*
428 has not been previously studied in the context of virus replication, its paralog *CCNA2* restricts
429 HCMV replication.[54] The largest group of genes represented in our screen were the PRAME
430 (preferentially expressed antigen in melanoma) family of leucine-rich repeat proteins. All five of
431 the PRAME family genes tested displayed some level of anti-viral activity, with *PRAMEF2*,
432 *PRAEMF8*, and *PRAMEF20* being among the top hits for both viruses. The only member of this
433 family in humans to have been studied mechanistically is *PRAME*, which can function as a
434 negative regulator of retinoic acid signaling.[55,56] However, *PRAME* does not appear to be a DSG
435 based on our analyses, and involvement in retinoic acid signaling has not been confirmed with
436 any other PRAME family members which share at most 53% peptide identity with *PRAME*. The
437 PRAME family is extensively duplicated in mammals. Additionally, both the PRAME family and
438 *LEUTX*, another top hit from this screen, have high allelic variation in humans and exhibit signs
439 of positive selection.[57-59] Our findings suggest that herpesvirus infections may have exerted
440 evolutionary selective pressure on the development and retention of these genes. We conclude
441 that many of the highly upregulated DSGs in trophoblasts possess strong anti-herpesvirus activity,
442 positioning them as compelling targets for future mechanistic studies to better understand their
443 roles in antiviral defense and potential therapeutic applications.

444 A detailed mechanism of how herpesvirus infection triggers *DUX4* expression has yet to be
445 reported. A recent study suggests that the HSV-1 immediate early genes RL2 (ICP0) and US1
446 (ICP4) are necessary and sufficient to induce DUX4 expression in HSV-1 infection.[51] In our
447 scRNAseq data of HSV-1 infection in TOs, we observed that 9 out of 50 HSV-1 genes were
448 expressed at comparable or higher levels in the DUX4-high cluster when compared to the HSV-
449 1-high cluster. All of these genes were immediate early (α), early (β), or unclassified HSV-1
450 transcripts. Thus, DUX4 expression being triggered by the activities of one or several immediate
451 early genes may explain this expression pattern. Importantly, US1 was not among the HSV-1
452 genes with higher expression in the DUX4-high cluster and the expression of RL2 was too low to

453 accurately conclude a pattern of expression between these clusters. Another observation that
454 may point to how DUX4 is controlled is that TOs respond to HCMV and HSV-1 with much higher
455 expression of both *DUX4* and downstream DSGs than matched maternal DOs. As trophoblasts
456 uniquely constitutively secrete IFN-λs,[9,15-17] we hypothesized that constitutive type-III IFN
457 signaling may modulate *DUX4* and DSG expression. However, knock-out of *IFNLR1* did not
458 decrease *DUX4* or DSG expression in TOs following HSV-1 infection, demonstrating that
459 constitutive type III IFN signaling does not influence this pathway. Nonetheless our data indicate
460 that TOs respond to herpesvirus infection with uniquely high expression of *DUX4* and DSGs,
461 which could be used in future studies to investigate how this pathway is induced and modulated
462 during herpesvirus infection.

463 Immune responses at the MFI must be tightly regulated to prevent damage to the developing
464 fetus. For example, in mice the type I IFN response, either induced by viruses or poly I:C, can
465 cause placental damage and lead to fetal demise.[11-13,60] Although RuV infection induced IFN and
466 ISG expression in TOs, demonstrating that IFN pathways can be activated in this model, HSV-1,
467 HSV-2, and HCMV infection had minimal impact on the expression of IFNs and ISGs. The
468 induction of DSGs may also have potential negative impacts on trophoblast function, raising the
469 possibility of trade-offs between antiviral defense and maintaining normal cellular processes.
470 Expression of DUX4 and six of the DSGs that were tested in our screen led to cell death in MRC5
471 cells, suggesting that expression of these genes could also be lethal in trophoblasts. Additionally,
472 although scRNAseq analysis of iDUX4 expression and HSV-1 infection revealed that all
473 trophoblast cell types can produce DSGs, the STB was one of the clusters that expressed the
474 highest levels of DSGs in response to HSV-1 infection. The STB is a critical trophoblast cell type
475 that participates in placental hormone secretion and nutrient, gas, and waste exchange. The
476 impacts of expression of a potently lethal gene in a polynuclear fused cell such as the STB are
477 unclear. DUX4 causes FSHD when aberrantly expressed in adult muscle cells—another
478 polynuclear fused cell type.[32,33] Finally, many DSGs are small molecule transporters, such as the

479 sodium phosphate transporter *SLC34A2* and the amino acid transporter *SLC36A2,*[61,62] which
480 were induced by 240-fold and 11-fold respectively by iDUX4 expression in TOs. In MRC5 cells
481 expression of SLC34A2 had a small impact on HCMV replication at one timepoint and no impact
482 on HSV-1 replication. However, an increase in expression of small molecule transporters could
483 disrupt the crucial functions of nutrient and waste exchange between the maternal and fetal blood
484 supplies across the STB. Thus, our data present the possibility that DUX4 expression in
485 trophoblasts following herpesvirus infection could contribute to impaired placental function.

486 The data presented here establish that DUX4 and its transcriptional targets, termed DSGs,
487 form the central response mechanism of trophoblasts to herpesvirus infection, underscoring their
488 critical role in the antiviral defense of these specialized cells. Like ISGs, DSGs are induced as
489 part of an antiviral defense mechanism and encode non-redundant effectors that likely target
490 distinct aspects of viral replication. However, the DUX4-DSG pathway appears uniquely adapted
491 for pregnancy, enabling a cell-intrinsic antiviral response in trophoblasts without activating
492 paracrine signaling that could disrupt maternal immune tolerance. Given the high prevalence of
493 herpesvirus exposure during pregnancy, this pathway may have evolved to balance effective
494 antiviral defense with the preservation of placental function and immune tolerance, ensuring
495 optimal pregnancy outcomes. These insights not only deepen our understanding of trophoblast
496 biology but also open new avenues for exploring therapeutic strategies to protect against
497 teratogenic viral infections.

Acknowledgements

This work was supported by NIH grants F32-AI183633 (JH), R01-AI173333 (CC), P01-AI129859 (CC), and R01-AI145828 (CC). We would like to acknowledge Phillip Kolb (University Hospital Freiburg), Rebecca Göttler (University Hospital Freiburg), Nat Moorman (University of North Carolina at Chapel Hill) and Bekah Dickmander (University of North Carolina at Chapel Hill) for assistance with HCMV propagation.

505 ## Materials and Methods

506 **Culture of trophoblast and decidua organoids.**

507 TO and DO lines employed in this study were derived from full-term placental tissue as
508 previously described.[17,63,64] Human tissue used in this study was obtained from Duke University
509 after approval from the Duke University Institutional Review Board and in accordance with the
510 guidelines of Duke University human tissue procurement. TOs were cultured by plating in domes
511 of Matrigel (Corning 356231) and maintained with term trophoblast organoid medium (tTOM)
512 [Advanced DMEM/F12 (Life Technologies, 12634010) supplemented with 1X B27 (Life
513 Technologies, 17504044), 1× N2 (Life Technologies, 17502-048), 10% FBS (vol/vol, Cytiva
514 HyClone, SH30070.03), 2 mM GlutaMAX™ supplement (Life Technologies, 35050061), 100
515 µg/ml Primocin (InvivoGen, ant-pm-1), 1.25 mM N-acetyl-L-cysteine (Sigma, A9165), 500 nM
516 A83-01 (Tocris, 2939), 1.5 µM CHIR99021 (Tocris, 4423), 50 ng/ml recombinant human EGF
517 (Gibco, PHG0314), 80 ng/ml recombinant human R-spondin 1 (R&D systems, 4645-RS-100), 100
518 ng/ml recombinant human FGF2 (Peprotech, 100-18C), 50 ng/ml recombinant human HGF
519 (Peprotech, 100-39), 10 mM nicotinamide (Sigma, N0636-100G), 5 µM Y-27632 (Sigma, Y0503-
520 1MG) and 2.5 µM prostaglandin E2 (PGE2, Tocris, 2296)].[17] DOs were maintained in Expansion
521 Medium (ExM) [Advanced DMEM/F12 (Life Technologies, 12634010) supplemented with 1X B27
522 without vitamin A (Life Technologies, 12587010), 1× N2 (Life Technologies, 17502-048), 2 mM
523 GlutaMAX™ supplement (Life Technologies, 35050061), 100 µg/ml Primocin (InvivoGen, ant-pm-
524 1), 1.25 mM N-acetyl-L-cysteine (Sigma, A9165), 500 nM A83-01 (Tocris, 2939), 50 ng/ml
525 recombinant human EGF (Gibco, PHG0314), 100 ng/mL recombinant human Noggin (Peprotech,
526 120-10C), 80 ng/ml recombinant human R-spondin 1 (R&D systems, 4645-RS-100), 100 ng/ml
527 recombinant human FGF-10 (Peprotech, 100-26), 50 ng/ml recombinant human HGF (Peprotech,
528 100-39), 10 mM nicotinamide (Sigma, N0636-100G), and 2.5 µM Y-27632 (Sigma, Y0503-
529 1MG)].[64] Organoid cultures were maintained in a humidified incubator with 5% CO_2 at 37°C, and
530 medium was renewed every 2-3 days. After 4-5 days in culture, organoids were grown in their

531 respective growth media without Y-27632. Organoids were passaged after 5-7 days in culture by
532 collecting Matrigel domes, digesting with TrypLE Express (Gibco, 12605-028) for 6-12 min at 37°C,
533 then mechanically dissociating into single cells and small fragments by manual pipetting.
534 Resulting cells were resuspended in Matrigel and plated as domes in 24-well tissue culture plates.
535

536 **Culture of cell lines and viruses.**

537 Lenti-X™ 293T cells (Takara, 632180), ARPE-19 cells (ATCC, CRL-2302) and Vero (ATCC,
538 CCL-81) cells were cultured in Dulbecco's minimal essential medium (DMEM) with 10% FBS and
539 1% penicillin/streptomycin (Gibco, 15140). MRC5 cells (ATCC, CCL-171) were cultured in DMEM
540 with 10% FBS, 1% penicillin/streptomycin (Gibco, 15140), 1x HyClone™ non-essential amino
541 acids (Cytiva, SH30238.01), 1 mM sodium pyruvate (Cytiva, SH30239.01). Cell lines were tested
542 for mycoplasma using the MycoStrip Mycoplasma Detection Kit (Invivogen, rep-mys-50).

543 mCherry-tagged HCMV TB40/E (a gift from N. Moorman[65]) was propagated by infecting ARPE-
544 19 (MOI ≅ 0.01) followed by extended incubation until >90% of cells showed cytopathic effect.
545 Growth on ARPE-19 cells was chosen to select for epithelial tropism. Both supernatant and cells
546 were harvested, cells were gently lysed by freeze/thaw, and pooled cell-associated and cell-free
547 virus was concentrated on a 20% sucrose cushion (20,000 rpm). Virus pellet was the
548 resuspended in sterile media before titration on MRC5 cells and ARPE-19 cells. The remaining
549 virus stocks were previously prepared, and aliquots were pulled from storage at -80°C for
550 experiments. GFP-UL25 HSV-1 KOS strain (a gift from F. Homa[66]),[8] HSV-2 333 strain (a gift from
551 H. Lazear), YFP-tagged VACV Western Reserve strain (a gift from S. Cherry),[8] RuV M33 strain
552 (ATCC, VR-315),[67] and ZIKV Paraiba-2015 strain (a gift from D. Watkins)[9] were all titrated on
553 Vero cells. Echo5 Noyce strain was titrated on HeLa cells [68].
554

555 **Virus infection in organoids**

556 Virus infections in organoids were performed either on coat-seeded cultures or in suspension.
557 Matrigel coats were generated by covering the bottom of a 48-well plate or 8-well chamber slide
558 with 20 uL of undiluted Matrigel, which was then allowed to polymerize for ~10 min. Dissociated
559 organoids were seeded on Matrigel coats following passage and allowed to grow in for 5-7 days
560 prior to infection. The coat-culturing method allows organoids to grow into 3D spherical structures,
561 but leaves the majority of the surface of each organoid unit exposed to the media rather than fully
562 imbedded in matrigel as is typical in Matrigel domes. Coat-seeded organoids were infected by
563 replacing the culturing media with inoculum (virus diluted in tTOM), incubating for 2 h at 37°C,
564 and then replacing the inoculum with fresh culturing media. Suspension infections were performed
565 by first releasing organoids from Matrigel domes using cell recovery solution (Corning, 354253)
566 at 4°C for 20-30 min. Organoids were pelleted by gravity, washed with PBS, and pelleted again.
567 Inoculum was then added to the released organoids. Infections were allowed to proceed for 2 h
568 at 37°C, agitating the culture every 30 min to keep the organoids from aggregating. Organoids
569 were then pelleted, resuspended in Matrigel, seeded in domes in 24-well plates, and submerged
570 with normal tTOM. Prior to infections, parallel wells of organoids were disrupted and counted to
571 calculate MOI. MOI for each experiment is specified in the results and figure legends.
572
573 **Lentivirus production.**
574 Lentiviral particles were produced in Lenti-X™ 293T cells (Takara, 632180) by transfection of
575 a lentiviral transfer plasmid along with psPAX2 (Addgene #12260) and pMD2.G (Addgene #12259)
576 packaging plasmids using TransIT®-293 transfection reagent (Mirus Bio, MIR 2700). 293T cells
577 were refed with intended target cell medium at 24 h post transfection. Supernatant was collected
578 at 48 h post transfection, filtered with 0.45 µm filter, then stored at -80°C prior to transduction of
579 target cells. psPAX2 and pMD2.G were gifts from Didier Trono. pCW57.1-DUX4-CA, used to
580 generate iDUX4 lentiviral particles, was a gift from Stephen Tapscott (Addgene #99281).[42]
581 Lentiviral plasmids for the overexpression of DSGs, CRISPR-Cas9-mediated editing of IFNLR1,

582 shRNAs, CRISPRi, and dominant-negative DUX4 overexpression were constructed by
583 VectorBuilder. Descriptions of these vectors along with vector IDs (that can be used to retrieve
584 detailed information on them) can be found in **Table S7**.
585

586 **Transduction and single-cell cloning of trophoblast organoids.**

587 Trophoblast organoids were transduced by first dissociating them into single-cell suspension
588 following the same protocol for passaging described above. The dissociated single cell
589 suspension was then incubated with filtered lentiviral supernatant and 8 µg/mL polybrene
590 overnight in an ultralow attachment plate at 37°C overnight. The transduced cell suspension was
591 resuspended in Matrigel and plated as domes. After 2-3 days of recovery, transduced cells were
592 selected for by supplementing the media with 2 ug/mL puromycin for 4-5 days. Single cell clones
593 of CRISPR-Cas9-edited organoids were generated by isolating and propagating individual
594 organoid units one passage after selection. This process takes advantage of the likelihood that
595 most organoids in Matrigel arise from a single or very few starting stem cells. Clonal organoid
596 lines were screened for knockout by isolating genomic DNA using GenElute Mammalian Genomic
597 DNA Purification Kit (Sigma, G1N350), amplifying the sgRNA target region using high-fidelity PCR,
598 and the sequencing the purified PCR product with sanger sequencing at GENEWIZ. The resulting
599 capillary electrophoresis traces were analyzed using the ICE analysis tool from Synthego. The
600 primers used to amplify the sgRNA target editing site in *IFNLR1* are listed in **Table S7**.
601

602 **Immunofluorescence and confocal microscopy.**

603 For immunofluorescence staining, organoids cultured in a layer of matrigel on 8-well chamber
604 slides. Organoids were fixed with 4% paraformaldehyde for 30 min, permeabilized with PBS with
605 0.5% Triton X-100 for 60 min, then blocked with 10% normal goat serum in PBS with 0.05%
606 TWEEN-20 for 60 min. Organoids were then incubated with primary antibody diluted in blocking
607 solution at 4°C overnight. Organoids were then washed with PBS and then incubated for 2 hr at

608 room temperature with Alexa Fluor-conjugated secondary antibodies. Organoids were washed
609 again with PBS and mounted in Vectashield (Vector Laboratories) containing 4′,6-diamidino- 2-
610 phenylindole (DAPI). The following antibodies were used for staining: DUX4 (Sigma, MABD116),
611 anti-V5-tag (Cell Signaling Technologies, #58009), Alexa Fluor 488 Goat anti-Mouse IgG
612 secondary antibody (Invitrogen, A11029), and Alexa Fluor 594 Goat anti-Rabbit IgG secondary
613 antibody (Invitrogen, A11037). Images were captured on an Olympus Fluoview FV3000 laser
614 scanning confocal microscope.
615
616 **Overexpression screen and automated microscopy.**
617 Lentivirus particles for constructs used in the screen were prepared as described above and
618 arrayed into 96-well plate format for this screen. MRC5 cells were seeded into 96-well plate format
619 at a density of 5 x 10^3 cells per well. The following day, the media on these cells was replaced
620 with MRC5 culturing medium supplemented with 16 µg/mL polybrene. 100 µL of the appropriate
621 lentivirus or mock media was added to each well. Transductions were performed in triplicate.
622 Transduction plates were then incubated statically at 37°C for 30 min, centrifuged at 800xg for 30
623 min, then incubated for an additional hour statically at 37°C. Transduction media was then
624 replaced with fresh culturing media. 24 h post transduction, the media was replaced with MRC5
625 culturing media supplemented with 2 µg/mL puromycin, and selection was allowed to proceed for
626 48 h. 72 h post transduction, selected cells were infected with HCMV TB40/E mCherry (5 x 10^4
627 particles/well), HSV-1 KOS GFP (5 x 10^3 particles/well), or mock media. Inoculums were applied
628 to cells for 2 h statically at 37°C. Inoculum was then replaced with fresh media. A Keyence BZ-
629 X810 all-in-one automated microscope was used to capture fluorescent and bright field images
630 at 10x magnification of every well at 24 h intervals for the duration of each experiment. Five fields
631 of images were captured per well. Cultures were maintained in a humidified, 37°C chamber during
632 imaging. Lentiviral constructs that led to complete cell death were excluded from further analysis.
633 This was defined by visual morphological assessment of bright field images (spherical cell body

634 and/or detachment) at 0 hpi and 24 hpi, which are timepoints at which cytopathic effects are not
635 observed by either virus in control conditions. Fluorescence quantification was performed using
636 BZ-X800 Image Analyzer (Keyence). Cell body areas were defined algorithmically using
637 brightfield images. Fluorescence intensity of the virally encoded tags were integrated within these
638 areas and then normalized to the total cellular area (in μm^2), yielding an RFU / μm^2 measurement
639 for each well at each timepoint.
640

641 **RNA extraction, qRT-PCR, and bulk RNAseq**

642 RNA for qRT-PCR and bulk RNAseq was purified using the Sigma GenElute total mammalian
643 RNA miniprep kit or the Qiagen RNAeasy Mini Kit following the manufacturer's instruction. cDNA
644 for qRT-PCR was generated from total RNA using iScript cDNA synthesis kit (Bio-Rad) following
645 the manufacturer's instructions. Quantitative PCR was performed using the iQ SYBR Green
646 Supermix (Bio-Rad, 1708882) on a CFX96 Touch Real-Time PCR Detection System (Bio-Rad).
647 Gene expression was determined based on a ΔCT method normalized to actin. Primers used for
648 qPCR can be found in **Table S7**.

649 Bulk RNAseq libraries were prepared by the Duke Center for Genomic and Computational
650 Biology using the KAPA mRNA HyperPrep Kit (Roche). Sequencing was performed as follows:
651 on a NovaSeq X Plus using 100 bp paired end sequencing for the diverse virus TO infection
652 experiment, on a NovaSeq 1000 using 100 bp paired end sequencing for the iDUX4 experiment,
653 and on a NextSeq 500 using 75 by paired end sequencing for the HSV-1 infection in matched TO
654 and DO experiment. The following datasets were downloaded from Sequence Read Archive (SRA)
655 and used in analyses: TO/DO infections with HCMV TB40/E and HCMV AD169r
656 (PRJNA869760),[17] iDUX4 expression in iPSCs (PRJNA377314),[31] and iDUX4 expression in
657 MB135 cells (PRJNA338591).[42]

658 RNAseq reads were aligned to the human genome (GRCh38) and the appropriate viral
659 genomes for each experiment using QIAGEN CLC Genomics Workbench (v24). Viral genomes

660 used in mapping are as follows: HCMV TB40/E (GenBank: MW439039.1), HSV-1 KOS (GenBank:
661 KT899744.1), HSV-2 333 (GenBank: LS480640.1), VACV WR (GenBank Assembly:
662 GCA_000860085.1), Echo5 Noyce (GenBank: AF083069.1), RuV M33 (GenBank: OM816674.1),
663 and ZIKV Paraíba (GenBank: KX280026.1). Differential gene expression analysis was performed
664 using DESeq2 package in R accounting for multiple donors in the statistical model.[36] PCA analysis
665 was performed using PCAtools package in R following correction for donor, experimental set, and
666 dpi batch effects using the ComBat function of the sva package.[69] Heatmaps were generated
667 using $\log_2$ normalized counts (an output from DESeq2) and the pheatmap package in R. Raw
668 data from the bulk RNAseq experiments reported here have been deposited into SRA
669 (PRJNA1213838).
670
671 **Dissociation of organoids for single cell RNAseq.**
672 Matrigel domes of organoids were resuspended into media [Advanced DMEM/F12 (Life
673 Technologies, 12634010) supplemented with 1% penicillin/streptomycin (Gibco, 15140), 10 mM
674 HEPES (Gibco, 15630-106), and 2 mM GlutaMAX™ supplement (Life Technologies, 35050061)]
675 and organoids were pelleted by centrifugation. The media was replaced by TrypLE Express
676 (Gibco, 12605-028), and organoids were digested at 37°C for 12 min. Organoids were pelleted
677 again and resuspended in 200 uL resuspension media and vigorously disrupted by manual
678 pipetting (~180 pipettes per min) for 3 min. The volume of the cell suspension was increased to 1
679 mL with PBS supplemented with 1% FBS. The cell suspension was then filtered through a 40 µm
680 filter cell strainer (Corning, 352098) using an additional 3 mL of PBS supplemented with 1% FBS
681 to wash the filter. Cells were pelleted by centrifugation and resuspended in 100 µL of PBS
682 supplemented with 1% FBS. Cells were counted and viability tested using trypan blue and
683 automated cell counting (Biorad TC20 automated cell counter). All samples had >1 x 10^6 live
684 cells/mL and viabilities >70%.
685

686 **Single-cell RNAseq library preparation and data analysis.**

687 Libraries were prepared from ~10,000 cells using 10x Genomics Single Cell 3' reagent kits (v2
688 chemistry, #CG00052) on a Chromium X instrument (10x Genomics) by the Molecular Genomics
689 Core at the Duke Molecular Physiology Institute. Sequencing was performed on a NovaSeq X
690 sequencer using a S4 flow cell which was predicted to yield around 71k reads / cell. Custom
691 genomes were constructed using the CellRanger package (v6.1.2, 10x Genomics) in Linux by
692 adding either the iDUX4 lentiviral vector sequence or the HSV-1 KOS genome (GenBank:
693 KT899744.1) to the human genome (GRCh38) as additional chromosomes. HSV-1 genes that
694 share a polyadenylation site (e.g. polycistronic or alternatively spliced transcripts) were grouped
695 into single features as they cannot be distinguished by the employed library preparation chemistry.
696 Post-processing and read alignment to these custom genomes were performed using the 10x
697 CellRanger package hosted through the 10x cloud analysis platform. Gene expression matrices
698 were analyzed using the Seurat (version 4) package in R.[70] Cells with between 2000 and 12000
699 uniquely expressed genes and between 4% and 25% mitochondrial reads were included for
700 downstream analysis. To eliminate batch effects, samples from different donors within the same
701 condition were normalized and integrated using the SCTransform and FindIntegrationFeatures
702 functions in Seurat while simultaneously regressing the following variables: percent mitochondrial
703 reads, percent ribosomal reads, percent X chromosome reads, percent Y chromosome reads,
704 number of features per cell, number of counts per cell, and percent HSV-1 reads (for the HSV-1
705 infection dataset) or DUX4/DSG score (for the iDUX4 dataset). The RNA assay was scaled and
706 normalized and ALRA-mediated imputation of the data was performed before subsequent
707 analyses.[71] Samples from separate conditions were then merged together using the Harmony
708 package in R.[72] Dimensional reduction was performed using the RunPCA function followed by the
709 RunUMAP function using the top 50 principle component dimensions. The FindNeighbors and
710 FindClusters commands were used to perform clustering at a resolution of 0.6. Determination of
711 an optimal resolution was aided by the clustree package.[73] Correlation between iDUX4 and all

712 other genes was performed using the Pearson correlation setting of the base cor() function in R.
713 Differential gene expression analysis was performed by retrieving the raw counts from each
714 cluster separated by original sample using the AggregateExpression function and then performing
715 DESeq2 analysis accounting for multiple donors in the statistical model.[36] HSV-1 transcripts were
716 classified as described in Dremel et al.[74]

717 To perform trajectory analysis of HSV-1 infected cells, the data were reanalyzed to only include
718 infected cells and to allow these cells to be ordered based on HSV-1 gene expression. Cells with
719 between 2000 and 12000 uniquely expressed genes, >10000 total reads, between 4% and 25%
720 mitochondrial reads, and >0.1% HSV-1 reads were included for downstream analysis. To
721 eliminate batch effects, samples from different donors were normalized and integrated using the
722 SCTransform and FindIntegrationFeatures functions in Seurat while simultaneously regressing
723 percent X chromosome reads, percent Y chromosome reads, and number of counts per cell.
724 Dimensional reduction was performed using the RunPCA function followed by the RunUMAP
725 function using the top 20 principle component dimensions. The FindNeighbors and FindClusters
726 commands were used to perform clustering at a resolution of 0.6. The SlingShot package in R
727 was used to predict pseudotime orders of infected cells from clusters identified in Seurat using a
728 defined starting cluster and undefined end clusters.[44] The fitGAM function of the tradeSeq
729 package in R was used to fit variable features, HSV-1 genes, and DSGs to a generalized additive
730 model along the predicted pseudotime trajectories.[75] The predictSmooth function was used to plot
731 the average expression of genes in cells along trajectories.

732 Raw data from the scRNAseq experiments reported here have been deposited into SRA
733 (PRJNA1213838).

734

735 **Statistics and reproducibility.**

736 All primary organoid-based experiments in this report have been replicated using independent
737 samples from organoid lines derived from multiple donors. Experiments in cell lines and cloned

organoids lines were performed with triplicate independent samples. Data in bar charts are presented as mean ± SD. In all graphics, each individual data point is shown when possible. Statistical significance was determined as described in the figure legends. All statistical analyses were performed using GraphPad Prism, unless otherwise specified (e.g. bulk RNAseq and scRNAseq). Unless otherwise specified, p values of <0.05 were considered to be statistically significant.

Figures and Legends

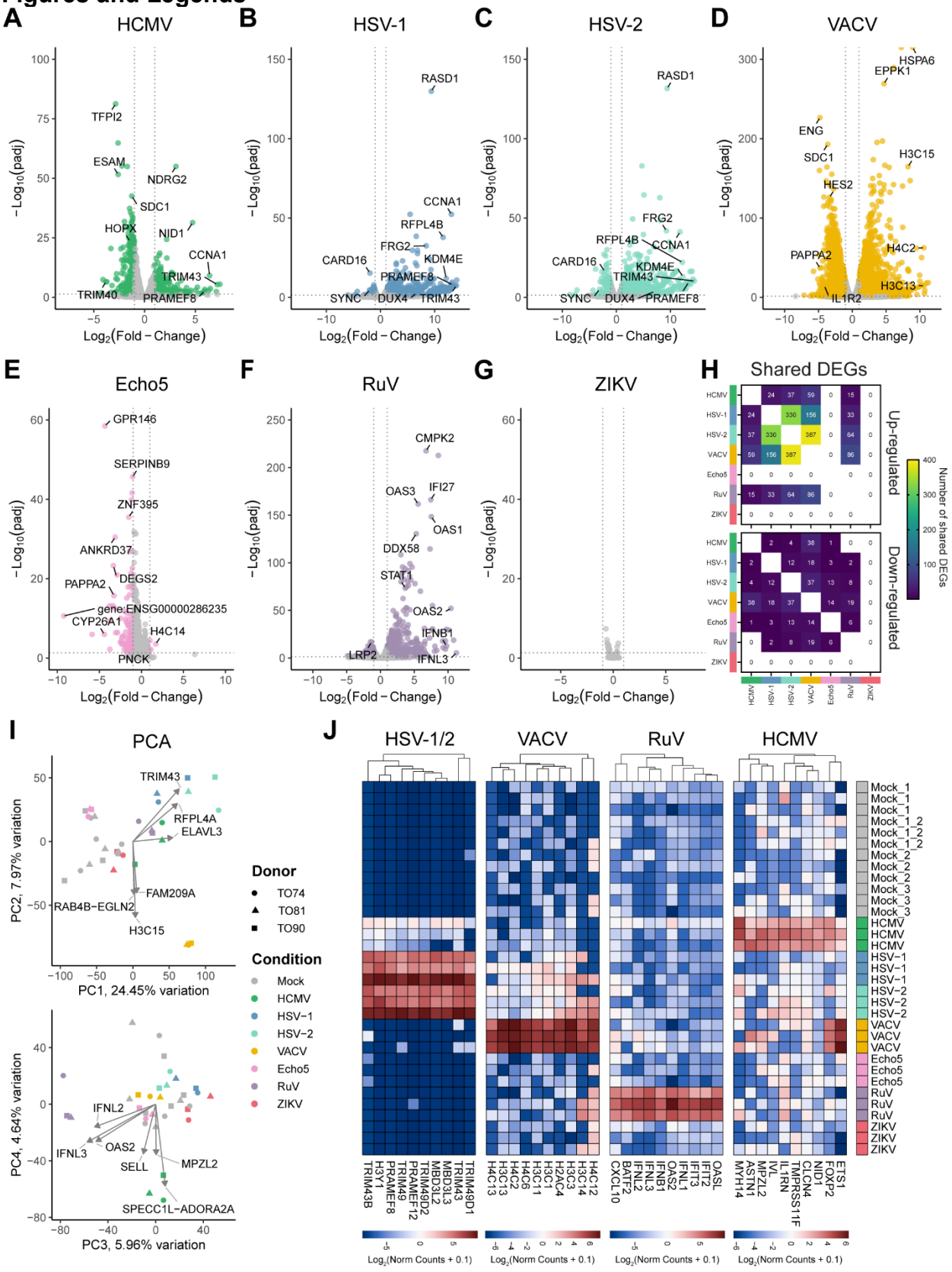

748 **Figure 1 | Trophoblast organoids respond distinctly to diverse viruses.** Trophoblast
749 organoids from three donors were infected with HCMV, HSV-1, HSV-2, VACV, Echo5, RuV, and
750 ZIKV at an MOI of 2. mRNA was purified and analyzed by bulk RNAseq. **(A-G)** Volcano plots
751 portraying the DEGs relative to mock samples. Colored circles represent significant DEGs
752 (Log2(fold-change) > 1 and adjusted *p*-value < 0.05). Gray circles represent genes whose
753 expression was not significantly impacted. Also see **Table S1**. **(H)** Heatmap showing the number
754 of shared DEGs between each infection condition. Genes that were found to be differentially
755 expressed between donors, timepoints, or experimental sets in the mock infected samples were
756 excluded from these tallies. **(I)** PCA of RNAseq data from each sample is portrayed in two graphs:
757 principle component 1 (PC1) vs PC2 (top) and PC3 vs PC4 (bottom). Shapes denote the donor a
758 sample came from, and color denotes the infection condition of the sample. **(J)** Heatmaps
759 portraying the genes that define the responses unique to virus types. Values are $\log_2$ normalized
760 counts from DESeq2 analysis plus a pseudo count of 0.1. Keys are at the bottom of each chart.
761 The scale is not constant between each heatmap. Red indicates higher expression and blue
762 indicates lower expression. Hierarchical clustering of genes is shown at the top.
763

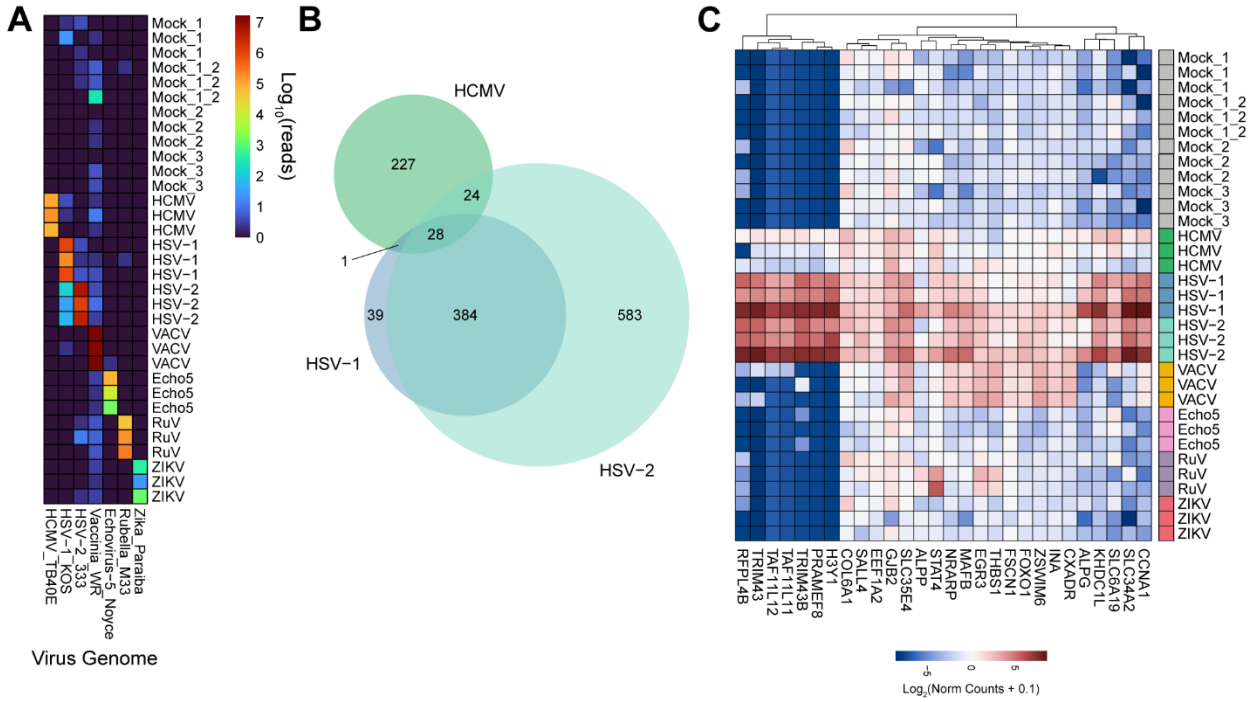

Figure S1 | Trophoblast organoids respond distinctly to diverse viruses. Trophoblast organoids from three donors were infected with HCMV, HSV-1, HSV-2, VACV, Echo5, RuV, and ZIKV at an MOI of 2. mRNA was purified and analyzed by RNAseq. **(A)** Heatmap portraying the $\log_{10}$ reads that map to each of the viral genomes. **(B)** Venn diagram denoting the number of shared DEGs between each of the herpesvirus infection conditions. **(C)** Heatmap portraying the genes that are induced by all three herpesviruses in TOs. Values are $\log_2$ normalized counts from DESeq2 analysis plus a pseudo count of 0.1. Key is at the bottom. Red indicates higher expression and blue indicates lower expression. Hierarchical clustering of genes is shown at the top.

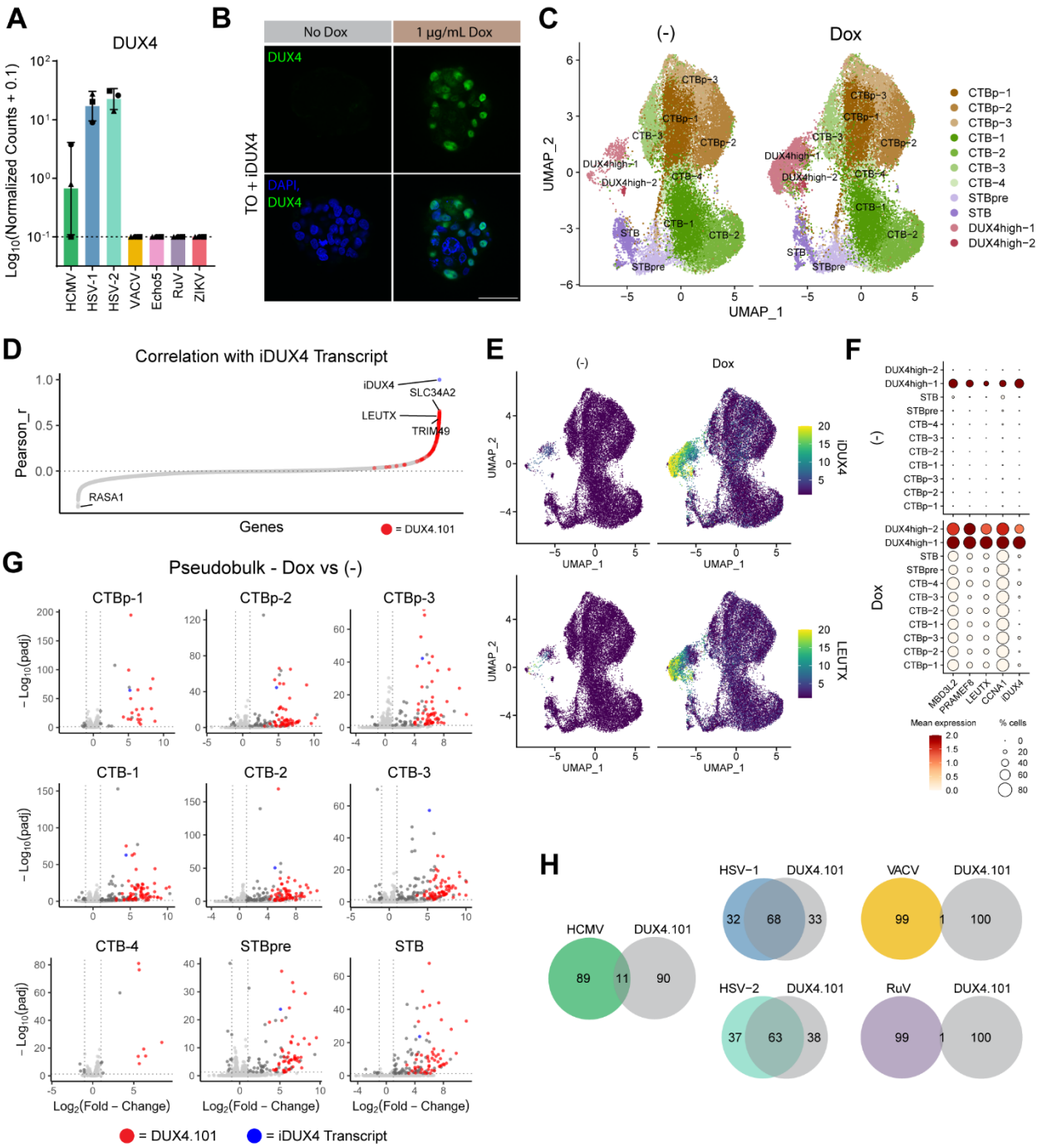

Figure 2 | Trophoblasts respond to herpesviruses with DUX4-stimulated genes. (A) Bar plot portraying the expression of *DUX4* in the RNAseq experiments from Figure 1. Shapes denote the donor of each data point. **(B)** Confocal micrographs of TOs engineered to express DUX4 under a doxycycline (Dox) inducible promoter. DUX4 is displayed in green and DAPI-stained nuclei are in blue. Scale bar = 100 µm. **(C)** UMAP of clusters from three donors of mock-treated TOs and three donors of Dox-treated TOs. Clusters are labeled as proliferative cytotrophoblasts (CTBp), cytotrophoblasts (CTB), pre-syncytiotrophoblasts (STBpre), syncytiotrophoblasts (STB), or DUX4-high cells. Multiple clusters from a single cell type are annotate with a -number after the cluster name. **(D)** Plot portraying the correlation (Pearson's r) between iDUX4 transcript and all other measured genes. Values are plotted in rank order. Genes that belong to the DUX4.101 list

are displayed as red circles. Also see **Table S2**. **(E)** Feature plots of iDUX4 (top) and the *LEUTX* (bottom) expression. Keys are shown to the right. **(F)** Dot plots showing the average expression (ALRA assay) and proportion of cells expressing selected DSGs and iDUX4 in each cluster separated into mock-treated samples (top) and Dox-treated samples (bottom). **(G)** Pseudobulk analysis identifying significant DEGs (Log2(fold-change) > 1 and adjusted *p*-value < 0.05) between Dox-treated samples and mock-treated samples. Results from all clusters other than the DUX4-high clusters are shown. Genes that belong to the DUX4.101 list are displayed as red circles and iDUX4 transcript is displayed as a blue circle. Also see **Table S4**. **(H)** Venn diagrams denoting the overlap between the top 100 DEGs upregulated by each virus and the DUX4.101 list.

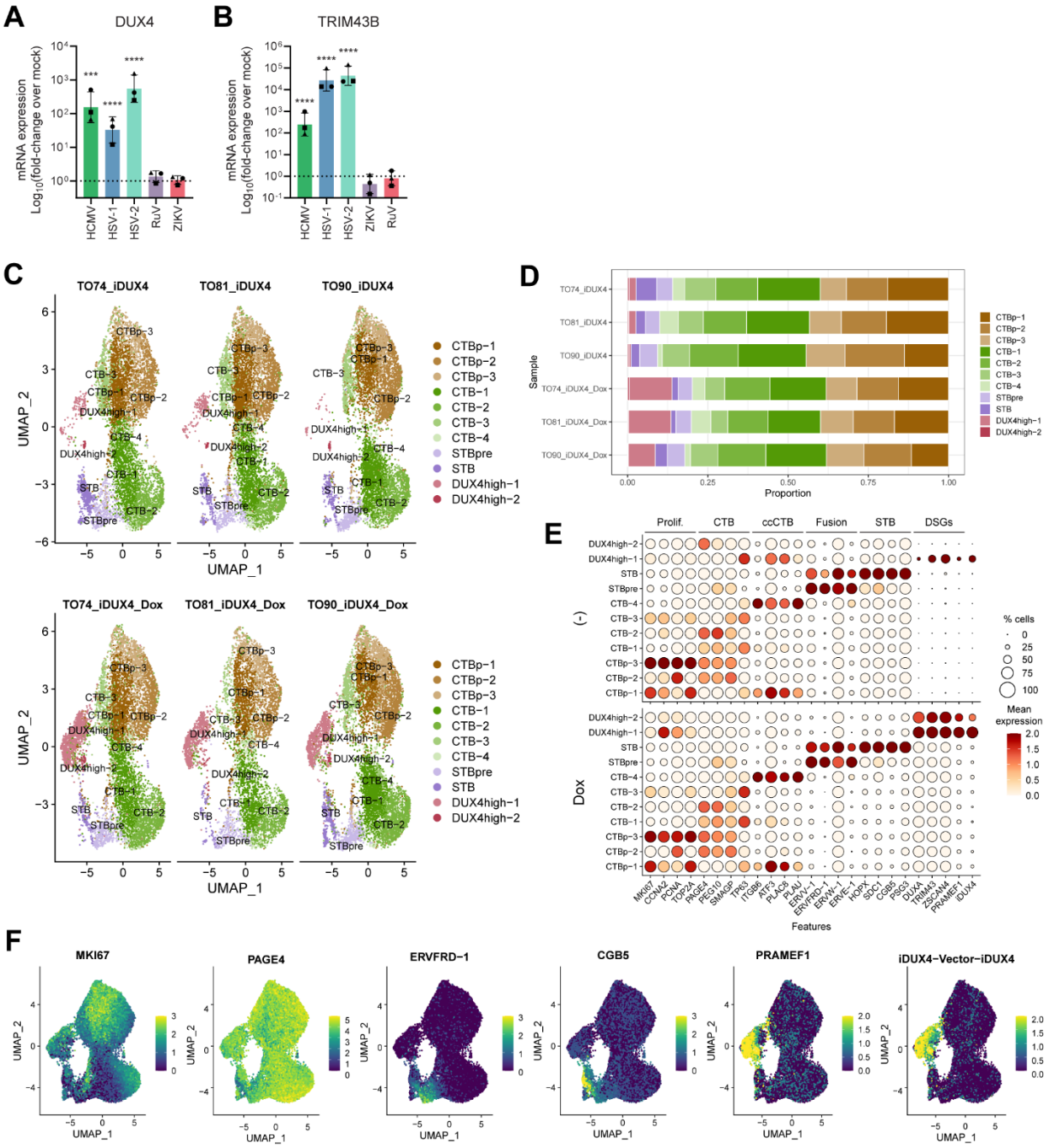

Figure S2 | Trophoblasts respond to herpesviruses with DUX4-stimulated genes. (A-B) Bar plot portraying the expression of *DUX4* and the DSG *TRIM43* as measured by qRT-PCR following the infection of TOs from three donors with HCMV, HSV-1, HSV-2, RuV, and ZIKV. Values are plotted as Log_{10}(fold-change over mock). Shapes denote the donor of each data point. Bars display mean ± SD. Statistical significance was determined by ANOVA with the Tukey multiple comparisons tests. *** $p < 0.001$, **** $p < 0.0001$. **(C)** UMAP of clusters from three donors of mock-treated TOs and three donors of Dox-treated TOs separated by sample. Clusters are labeled as proliferative cytotrophoblasts (CTBp), cytotrophoblasts (CTB), pre-syncytiotrophoblasts (STBpre), syncytiotrophoblasts (STB), or DUX4-high cells. Multiple clusters

808 from a single cell type are annotate with a -number after the cluster name. **(D)** Comparison of the
809 proportion of cells that belong to each cluster by sample. **(E)** Dot plots showing the average
810 expression (ALRA assay) and proportion of cells expressing selected genes in each cluster
811 separated into mock-treated samples (top) and Dox-treated samples (bottom). The selected
812 genes are established markers of proliferation, CTBs, cell column CTBs (ccCTBs), fusion, the
813 STB, and DSGs. **(F)** Feature plots of representative markers of each cell type.
814

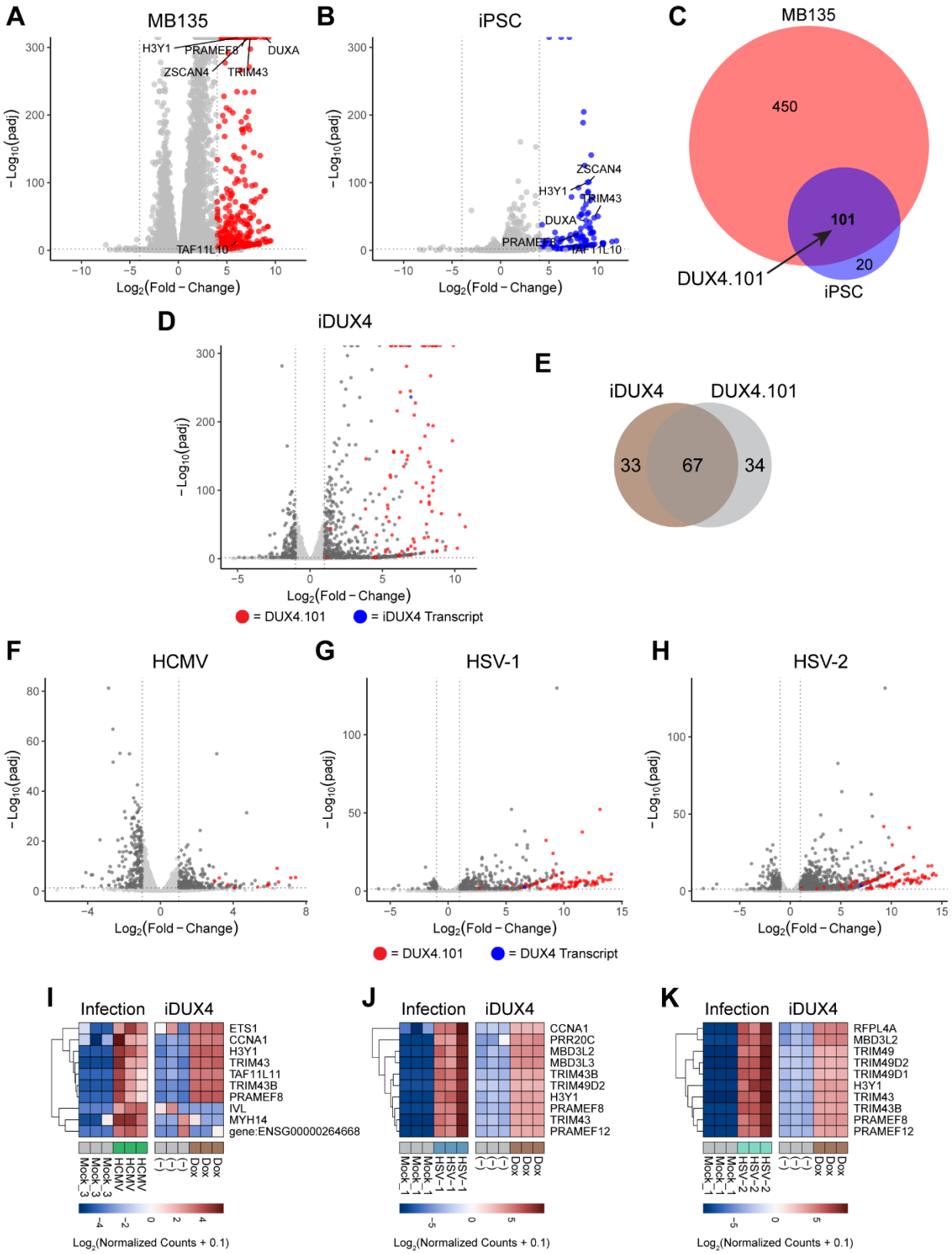

Figure S3 | Trophoblasts respond to herpesviruses with DUX4-stimulated genes. (A-B) Volcano plots portraying the DEGs upon DUX4 expression in (A) MB135 cells or (B) iPSCs. Colored circles represent significant DEGs (Log2(fold-change) > 4 and adjusted *p*-value < 0.01).

Gray circles represent genes whose expression did not meet these criteria. Also see **Table S3**. **(C)** Venn diagram denoting the overlap between the genes induced by DUX4 expression in MB135 cells and iPSCs. These 101 genes constitute the DUX4.101 list used throughout the paper as canonical DSGs that are expressed in divergent cell types. **(D)** TOs engineered to express DUX4 under a doxycycline (Dox) inducible promoter. RNAseq was performed on mock-treated and Dox-treated samples. Volcano plot portrays the DEGs upon DUX4 expression in TOs. Genes that belong to the DUX4.101 list are displayed as red circles and iDUX4 transcript is displayed as a blue circle. Significant DEGs (Log2(fold-change) > 1 and adjusted *p*-value < 0.05) are depicted in dark gray. Light gray was used to depict genes that did not meet these criteria. Also see **Table S3**. **(E)** Venn diagram denoting the overlap between the top 100 DEGs upregulated by iDUX4 expression in TOs and the DUX4.101 list of DSGs. **(F-H)** Volcano plots portraying the DEGs upon HCMV (F), HSV-1 (G), or HSV-2 (H) infection in TOs from Figure 1. Genes that belong to the DUX4.101 list are displayed as red circles and *DUX4* transcript is displayed as a blue circle. Significant DEGs (Log2(fold-change) > 1 and adjusted p-value < 0.05) are depicted in dark gray. Light gray was used to depict genes that did not meet these criteria. **(I-K)** Heatmaps comparing the expression of the top 10 genes induced by HCMV (I), HSV-1 (J), or HSV-2 (K) infection in TOs to the expression of those same genes following iDUX4 expression in TOs. Values are $\log_2$ normalized counts from DESeq2 analysis plus a pseudo count of 0.1. Keys are at the bottom of each chart. The scale is not constant between each heatmap. Red indicates higher expression and blue indicates lower expression. Hierarchical clustering of genes is shown to the left.

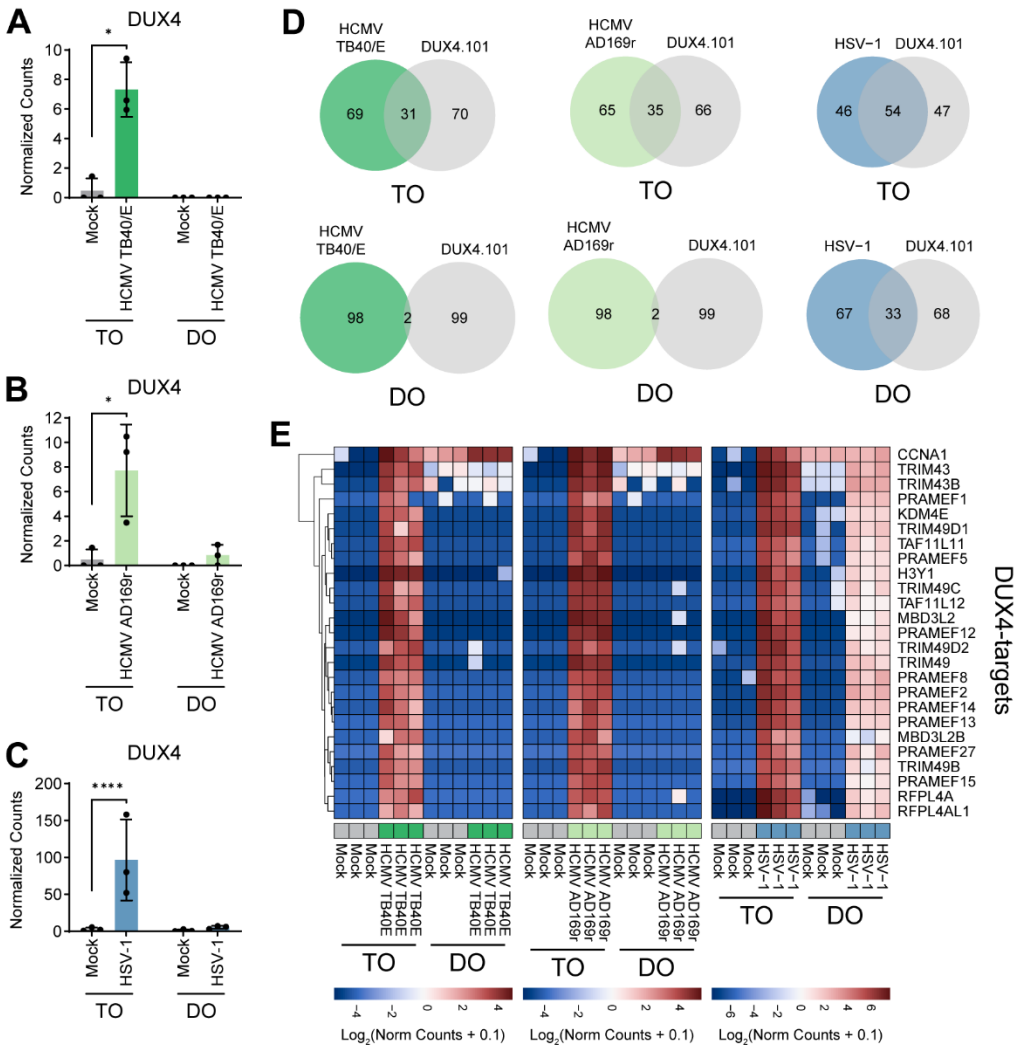

Figure 3 | DUX4-stimulated genes are induced to higher levels in trophoblast organoids than maternal-derived decidua epithelial organoids. RNAseq analysis was employed to assess if TOs and DOs differentially express DUX4 or DSGs when infected with HCMV TB40/E, HCMV AD169r, and HSV-1 (MOI of 5). Also see **Table S5**. **(A-C)** Bar plots portraying the expression of *DUX4* in TOs and DOs in mock-treated samples or those infected with HCMV TB40/E (A), HCMV AD169r (B), and HSV-1 (C). Each individual normalized count value is displayed. Bars represent mean ± SD. Statistical significance was determined using DESeq2 differential expression analysis. * $p < 0.05$, **** $p < 0.0001$. **(D)** Venn diagrams denoting the overlap between the top 100 DEGs upregulated by each virus and the DUX4.101 list with TO infections on the top and DO infections on the bottom. **(E)** Heatmaps portraying the expression of canonical DSGs following infection of TOs and DOs with HCMV TB40/E, HCMV AD169r, and HSV-1. Values are $\log_2$ normalized counts from DESeq2 analysis plus a pseudo count of 0.1. Keys are at the bottom of each chart. The scale is not constant between each heatmap. Red indicates higher expression and blue indicates lower expression. Hierarchical clustering of genes is shown on the left.

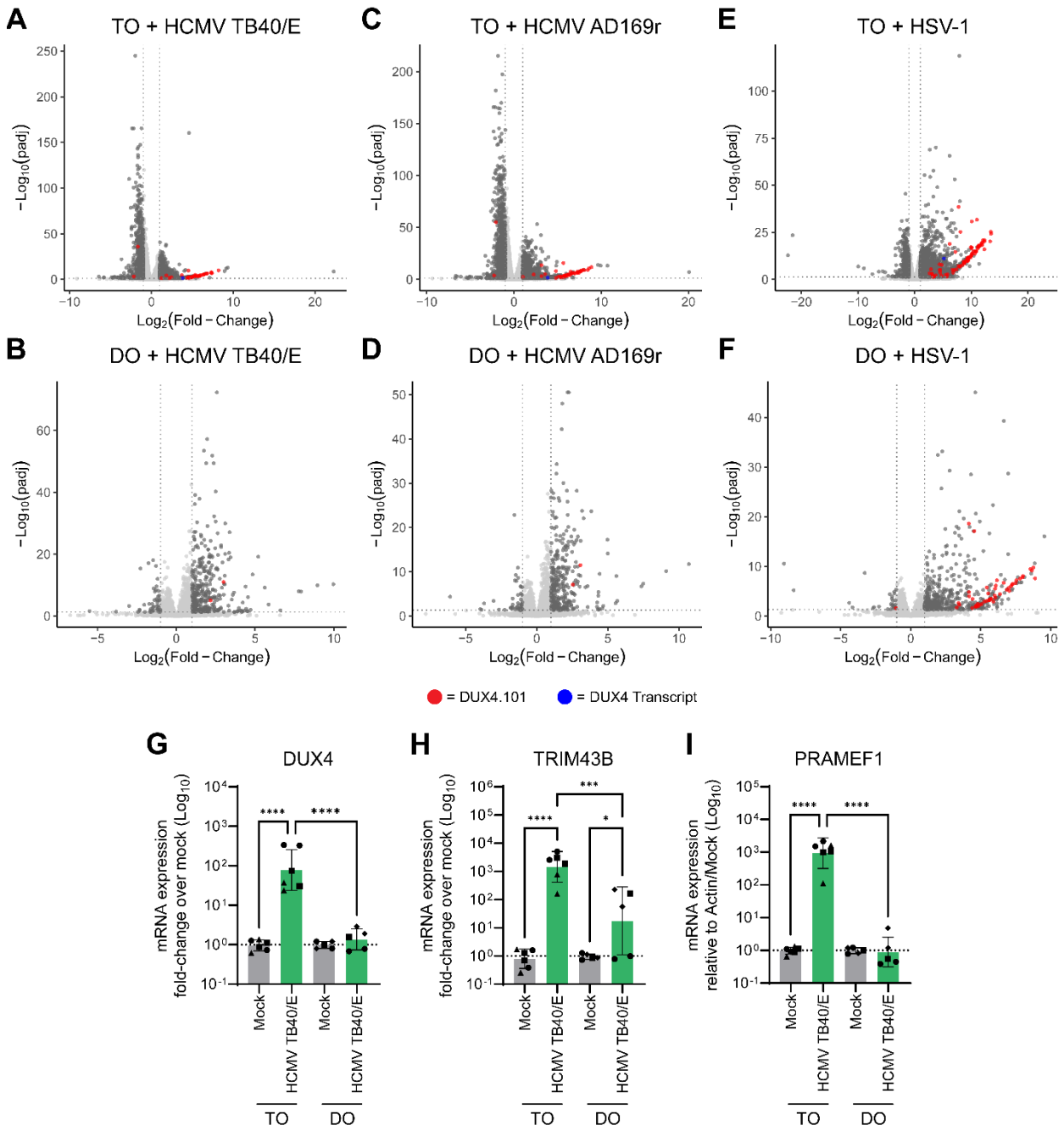

Figure S4 | DUX4-stimulated genes are induced to higher levels in trophoblasts than maternal decidual epithelial cells. RNAseq analysis was employed to assess if TOs and DOs differentially express DUX4 or DSGs when infected with HCMV TB40/E, HCMV AD169r, and HSV-1. Also see **Table S5**. **(A-F)** Volcano plots portraying the DEGs upon HCMV TB40/E (A-B), HCMV AD169r (C-D), or HSV-1 (E-F) infection in TOs (top) and DOs (bottom). Genes that belong to the DUX4.101 list are displayed as red circles and DUX4 transcript is displayed as a blue circle. Significant DEGs (Log2(fold-change) > 1 and adjusted p-value < 0.05) are depicted in dark gray. Light gray was used to depict genes that did not meet these criteria. **(G-I)** TOs and DOs from three donors each (two matched and one unique to each) were infected with HCMV TB40/E and qRT-PCR was used to measure the expression of *DUX4* and the DSGs *TRIM43B* and *PRAMEF1*. Values are plotted as Log_{10}(fold-change over mock). Shapes denote the donor of each data point.

869 Bars display mean ± SD. Statistical significance was determined by ANOVA with the Tukey
870 multiple comparisons tests. * $p < 0.05$, *** $p < 0.001$, **** $p < 0.0001$.
871

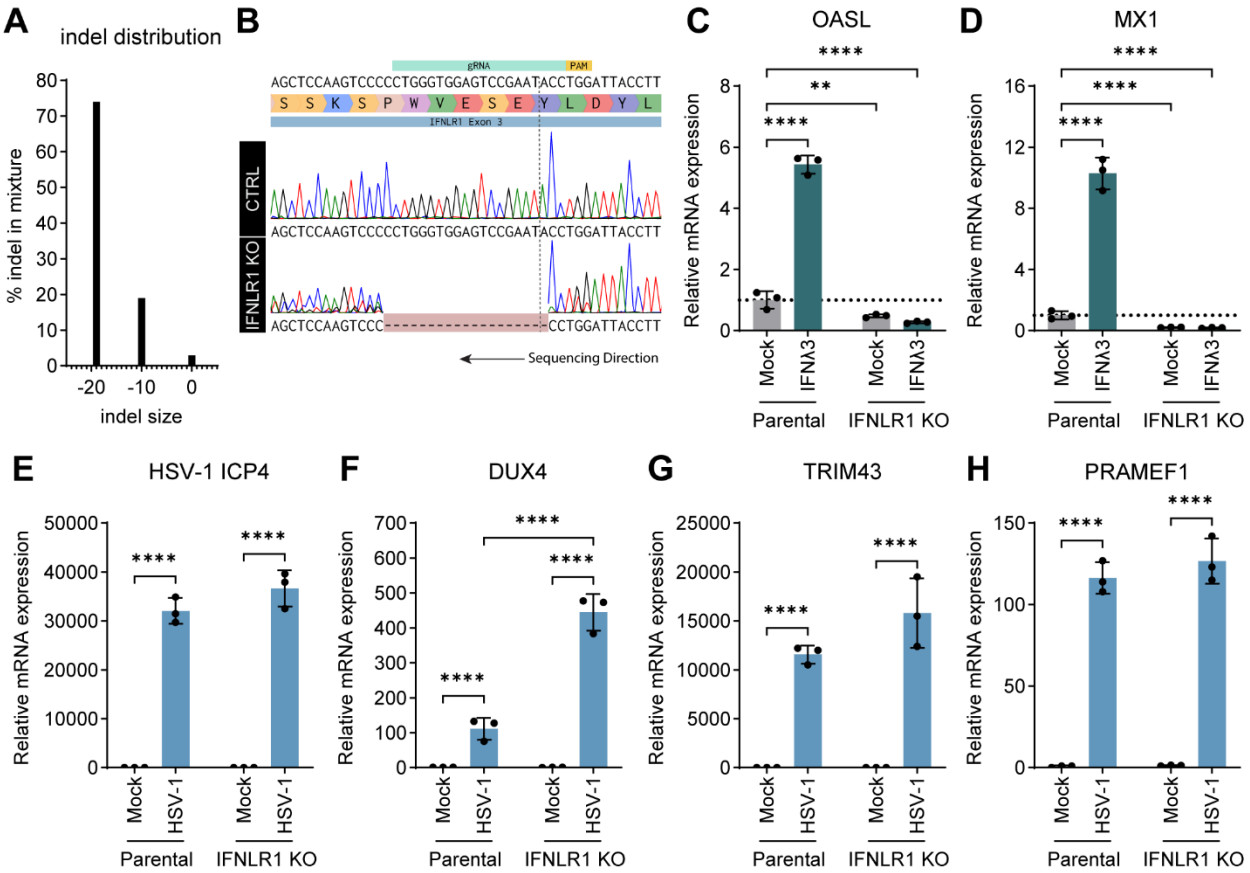

Figure 4 | Expression of DUX4 and DSGs are not dependent on constitutive type-III IFN signaling. TOs were transduced with lentiviral vectors engineered to express Cas9 and an sgRNA to target exon three of the human IFNLR1 locus. Single cell cloning was used to isolate homogenous organoid lines. PCR amplicons of the sgRNA target site were sent for sanger sequencing and analyzed using the Synthego ICE tool. **(A)** Predicted indel distribution of the IFNLR1 KO clone. **(B)** Sanger sequencing traces of the IFNLR1 KO clone aligned to a control sequencing trace. Sequencing proceeded from right to left as the traces are displayed. **(C-D)** IFNLR1 KO and parental organoids were mock-treated or treated with 5 ng/μL IFNλ3. qRT-PCR was used to measure the expression of the ISGs *OASL* and *MX1*. **(E-H)** IFNLR1 KO and parental organoids were infected with HSV-1 to induce DUX4/DSGs. qRT-PCR was used to measure the expression of HSV-1 ICP4, *DUX4*, *TRIM43B*, and *PRAMEF1*. Values are plotted as expression relative to parental mock and each individual data point is displayed. Bars display mean ± SD. Statistical significance was determined by ANOVA with the Tukey multiple comparisons tests. * $p < 0.05$, ** $p < 0.01$, **** $p < 0.0001$.

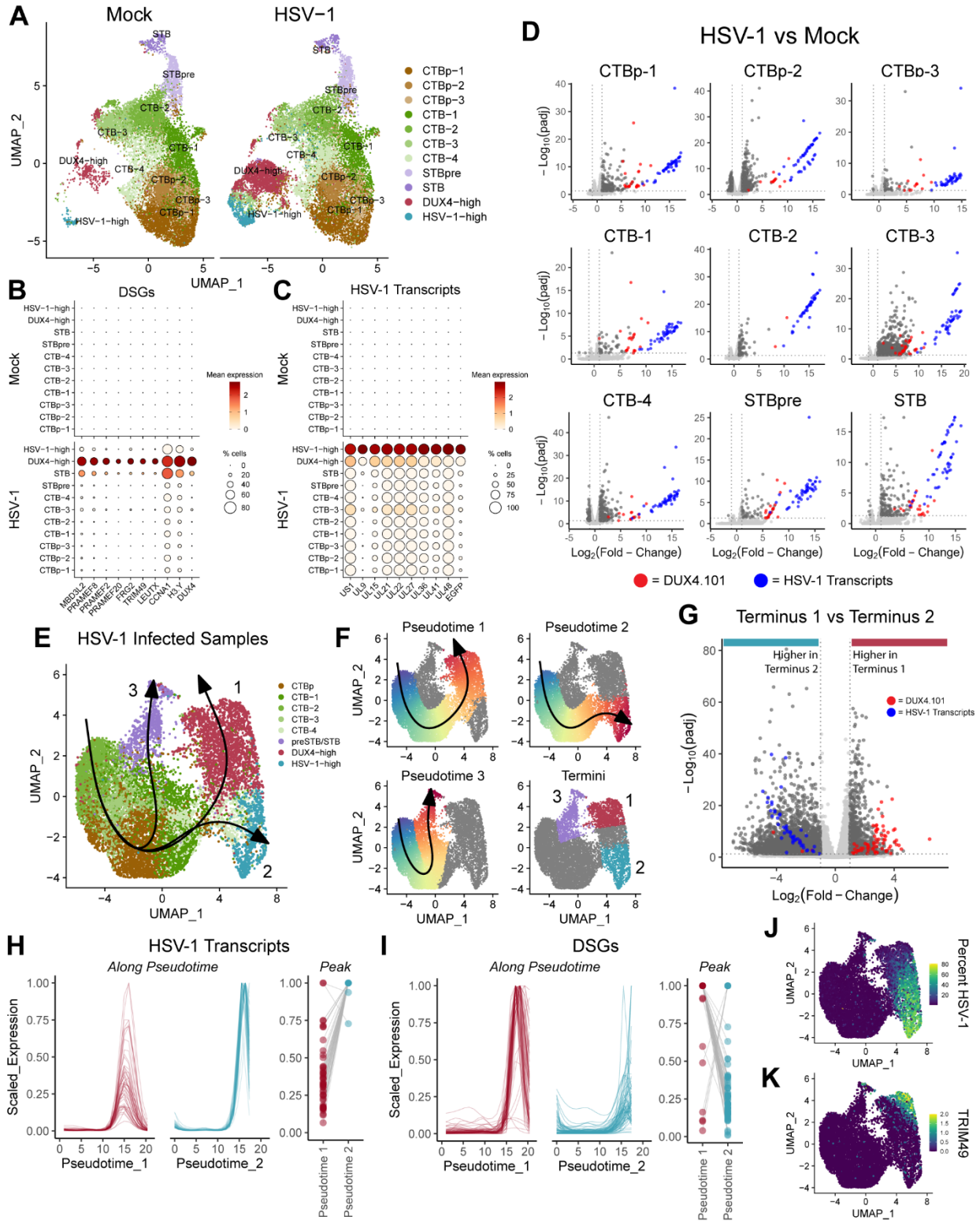

Figure 5 | DUX4-stimulated genes define a low viral gene expression trajectory in HSV-1-infected trophoblast organoids. HSV-1-infected and mock-infected organoids from two donors (2x TO74 samples and 1x TO84 sample each) were analyzed by scRNAseq. **(A)** UMAP of clusters from all mock-infected and all HSV-1-infected TOs separated by infection status. Clusters are

labeled as proliferative cytotrophoblasts (CTBp), cytotrophoblasts (CTB), pre-syncytiotrophoblasts (STBpre), syncytiotrophoblasts (STB), DUX4-high cells, or HSV-1-high cells. Multiple clusters from a single cell type are annotate with a -number after the cluster name. **(B-C)** Dot plots showing the average expression (ALRA assay) and proportion of cells expressing selected DSGs (B) and HSV-1 transcripts (C) in each cluster separated into mock-infected samples (top) and HSV-1-infected samples (bottom). **(D)** Pseudobulk analysis identifying significant DEGs (Log2(fold-change) > 1 and adjusted *p*-value < 0.05) between HSV-1-infected samples and mock-infected samples. Results from all clusters other than the DUX4-high and HSV-1-high clusters are shown. Genes that belong to the DUX4.101 list are displayed as red circles and HSV-1 transcripts are displayed as blue circles. Also see **Table S6**. **(E)** UMAP of re-clustered cells from HSV-1 infected samples with >0.1% HSV-1 reads. Clusters are labeled as CTBp, CTB, preSTB/STB, DUX4-high, or HSV-1-high. Multiple clusters from a single cell type are annotate with a -number after the cluster name. Slingshot trajectories are superimposed and numbered. **(F)** Featureplots of the pseudotime values (0-100) assigned to each cell along each trajectory (top and lower left). Featureplot showing the cells that were part of the final 15% of cells in a trajectory and designated as part of a trajectory terminus (lower right). **(G)** Pseudobulk analysis identifying significant DEGs (Log2(fold-change) > 1 and adjusted *p*-value < 0.05) between terminus 1 and terminus 2. Genes that belong to the DUX4.101 list are displayed as red circles and HSV-1 transcripts are displayed as blue circles. **(H-I)** Plots of the average expression (scaled to between 0 and 1) of all HSV-1 transcripts (H) and all DSGs (I) along pseudotime 1 and pseudotime 2. Relative peak expression of each HSV-1 transcript (H) and each DSG (I) along each trajectory is shown in a plot to the right. **(J-K)** Featureplots showing percent HSV-1 reads (J) and the expression of the DSG *TRIM49* (K).

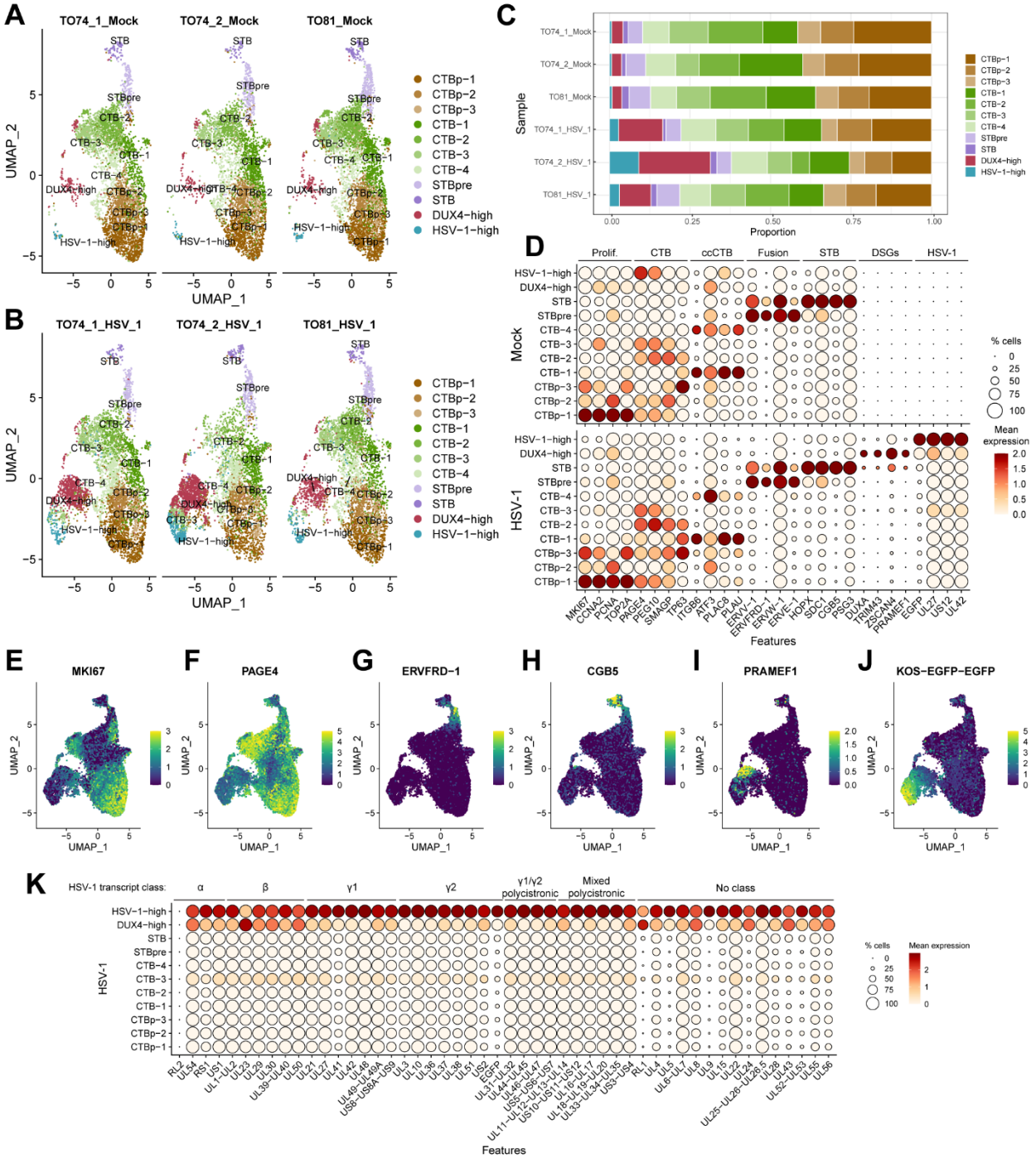

Figure S5 | DUX4-stimulated genes define a low viral gene expression trajectory in HSV-1-infected trophoblast organoids. HSV-1-infected and mock-infected organoids from two donors (2x TO74 samples and 1x TO84 sample each) were analyzed by scRNAseq. **(A-B)** UMAP of clusters from all mock-infected (A) and all HSV-1-infected (B) TOs separated by sample. Clusters are labeled as proliferative cytotrophoblasts (CTBp), cytotrophoblasts (CTB), pre-syncytiotrophoblasts (STBpre), syncytiotrophoblasts (STB), DUX4-high cells, or HSV-1-high cells. Multiple clusters from a single cell type are annotate with a -number after the cluster name. **(C)** Comparison of the proportion of cells that belong to each cluster by sample. **(D)** Dot plots showing the average expression (ALRA assay) and proportion of cells expressing selected genes in each

927 cluster separated into mock-infected samples (top) and HSV-1-infected samples (bottom). The
928 selected genes are established markers of proliferation, CTBs, cell column CTBs (ccCTBs), fusion,
929 the STB, DSGs, and HSV-1 transcripts. **(E-J)** Feature plots of representative markers of each cell
930 type. **(K)** Dot plots showing the average expression (ALRA assay) and proportion of cells
931 expressing all HSV-1 transcripts in each cluster. HSV-1 transcripts are organized into α
932 (immediate early), β (early), γ1 (leaky late), γ2 (true late), γ1/γ2 polycistronic/alternatively spliced,
933 mixed polycistronic/alternatively, and no class.
934

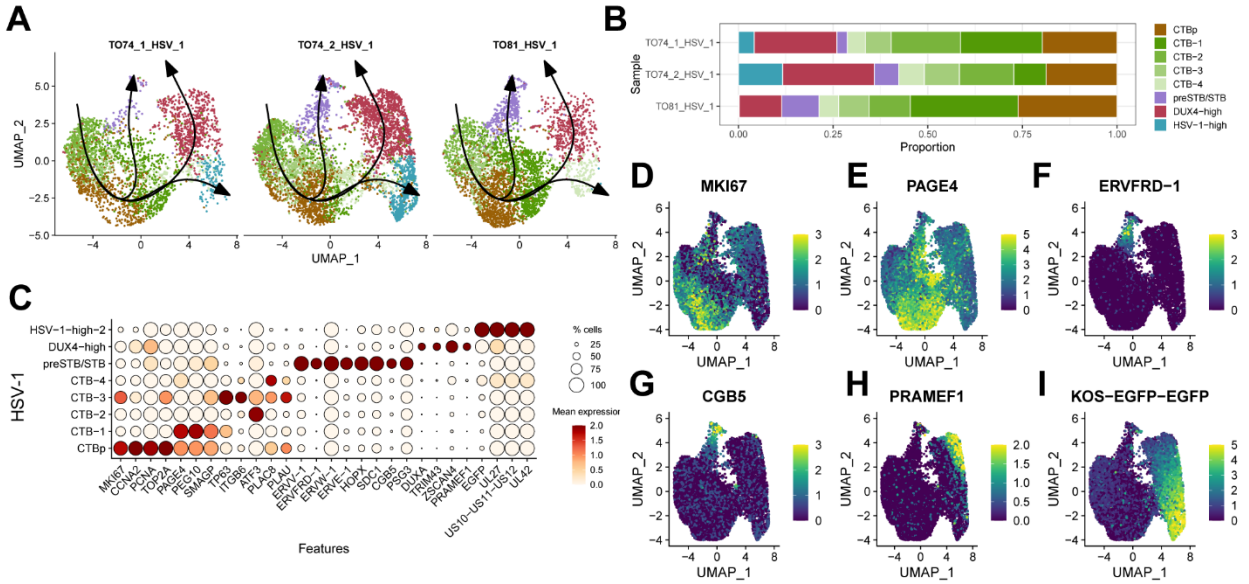

Figure S6 | DUX4-stimulated genes define a low viral gene expression trajectory in HSV-1-infected trophoblast organoids. (A) UMAP of re-clustered cells from HSV-1 infected samples with >0.1% HSV-1 reads separated by sample. Clusters are labeled as CTBp, CTB, preSTB/STB, DUX4-high, or HSV-1-high. Multiple clusters from a single cell type are annotate with a -number after the cluster name. Slingshot trajectories are superimposed. **(B)** Comparison of the proportion of cells that belong to each cluster by sample. **(C)** Dot plots showing the average expression (ALRA assay) and proportion of cells expressing selected genes in each cluster. The selected genes are established markers of proliferation, CTBs, cell column CTBs (ccCTBs), fusion, the STB, DSGs, and HSV-1 transcripts. **(D-I)** Feature plots of representative markers of each cell type.

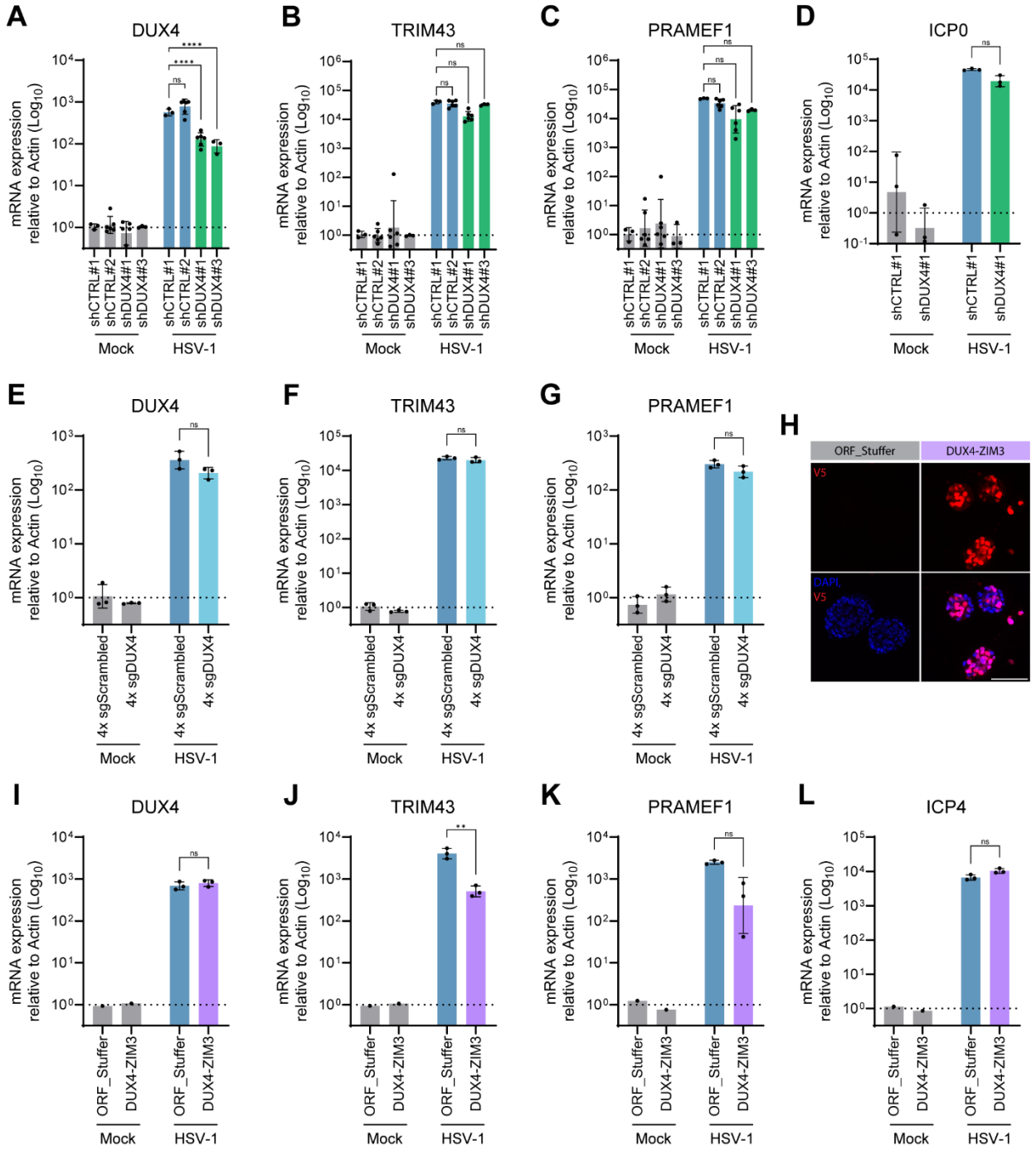

Figure S7 | DUX4 knockdown strategies in TOs. (A-D) TOs were engineered to express control (shCTRL) or *DUX4*-targeting (shDUX4) shRNAs. Engineered TOs were infected with HSV-1 at an MOI of 5, and RNA was collected at 24 hpi. qRT-PCR was used to measure the expression of *DUX4* (A), *TRIM43* (B), *PRAMEF1* (C), and HSV-1 ICP4 (D). **(E-G)** TOs were engineered to expresses dCas9-KRAB-MeCP2 (used for CRISPRi) along with either 4 scrambled sgRNAs (4x sgScrambled) or 4 sgRNAs targeting the transcription start site of DUX4 (4x sgDUX4). Engineered TOs were infected with HSV-1 at an MOI of 5, and RNA was collected at 24 hpi. qRT-PCR was used to measure the expression of *DUX4* (E), *TRIM43* (F), and *PRAMEF1* (G). **(H-L)** TOs were engineered to express a control vector (ORF_Stuffer) or a dominant-negative DUX4

957 construct with the transcriptional activation domain of DUX4 replaced with the KRAB domain of
958 ZIM3 along with a V5 tag (DUX4-ZIM3). Confocal micrographs. V5 staining is in red and DAPI-
959 stained nuclei are in blue. Scale bar = 100 μm (H). Engineered TOs were infected with HSV-1 at
960 an MOI of 5, and RNA was collected at 24 hpi. qRT-PCR was used to measure the expression of
961 *DUX4* (I), *TRIM43* (J), *PRAMEF1* (K), and HSV-1 ICP0 (L).
962

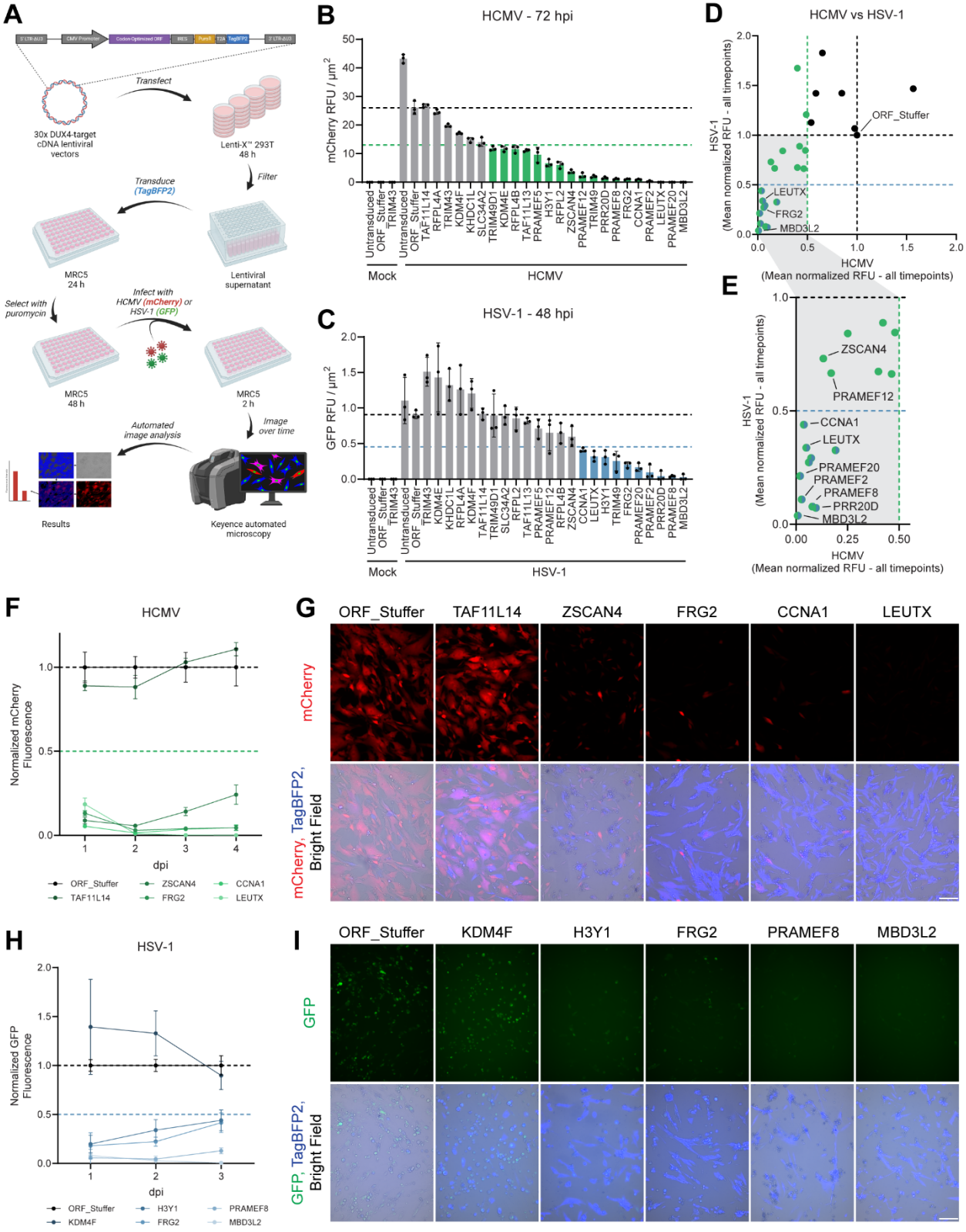

Figure 6 | DUX4-stimulated genes exert anti-herpesvirus activity, (A) Schematic representing the screening method in MRC5 cells. **(B-C)** Bar graphs depicting representative timepoints for HCMV (B; 72 hpi) and HSV-1 (C; 48 hpi). Black circles represent each individual datapoint. Bars

967 display mean ± SD. **(D)** Mean normalized relative fluorescence units (RFU) from HCMV in cells
968 expressing each DSG plotted against the mean normalized RFU from HSV-1 in cells expressing
969 each DSG (mean of all timepoints). **(E)** Zoomed in view of panel (D). **(F-G)** Representative DSGs
970 for HCMV: one with minimal impact and four top hits. Normalized mCherry fluorescence from
971 HCMV for these genes at all timepoints (F). Dots and error bars display mean ± SD. Widefield
972 micrographs of representative fields from 72 hpi. mCherry is portrayed in red in the top row, and
973 merged mCherry (red), TagBFP2 (blue), and brightfield (grayscale) is portrayed in the bottom row
974 (G). Scale bars = 200 µm. **(H-I)** Representative DSGs for HSV-1: one with minimal impact and
975 four top hits. Normalized GFP fluorescence from HSV-1 for these genes at all timepoints (H). Dots
976 and error bars display mean ± SD. Widefield micrographs of representative fields from 48 hpi.
977 GFP is portrayed in green in the top row, and merged GFP (green), TagBFP2 (blue), and
978 brightfield (grayscale) is portrayed in the bottom row (I). Scale bars = 200 µm. Black dashed lines
979 in graphs represent the mean expression of ORF_Stuffer. Colored dashed lines represent 0.5x
980 the black line.
981

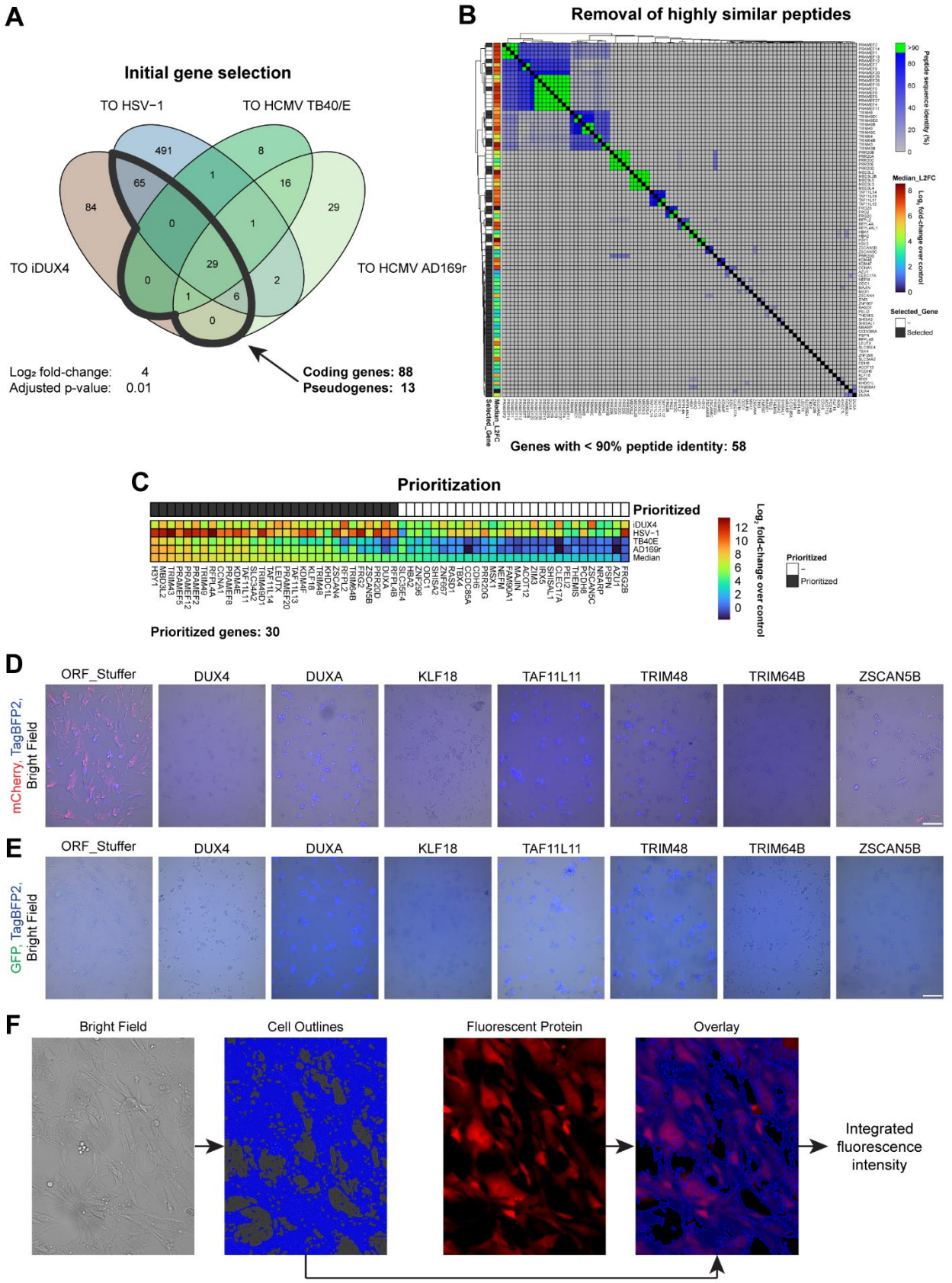
A
Initial gene selection
TO HSV−1
TO HCMV TB40/E
TO iDUX4
TO HCMV AD169r
491
8
65
1
16
84
29
0
1
29
0
2
1
6
0
Log₂ fold-change: 4
Adjusted p-value: 0.01
Coding genes: 88
Pseudogenes: 13
B
Removal of highly similar peptides
Peptide sequence identity (%)
Median_L2FC
Log₂ fold-change over control
Selected_Gene
Selected
Genes with < 90% peptide identity: 58
C
Prioritization
Prioritized
iDUX4
HSV−1
TB40E
AD169r
Median
Log₂ fold-change over control
Prioritized genes: 30
D
ORF_Stuffer
DUX4
DUXA
KLF18
TAF11L11
TRIM48
TRIM64B
ZSCAN5B
mCherry, TagBFP2, Bright Field
E
GFP, TagBFP2, Bright Field
F
Bright Field
Cell Outlines
Fluorescent Protein
Overlay
Integrated fluorescence intensity

982

983 **Figure S8 | DUX4-stimulated genes exert anti-herpesvirus activity. (A)** Venn diagram
984 depicting the overlap between DEGs induced by iDUX4 expression or HSV-1, HCMV TB40/E, or
985 HCMV AD169r infection in TOs (Log_2(fold-change) > 4 and adjusted p-value < 0.01). Thick line
986 highlights the selected genes. **(B)** Heatmap depicting the percent peptide sequence identity
987 between genes selected in (A). Genes with >90% peptide sequence identity are highlighted in
988 green. Median log_2 fold-change over control from iDUX4 expression and HSV-1, HCMV TB40/E,
989 and HCMV AD169r infection in TOs are displayed to the left. Genes selected for further
990 consideration are marked in gray to the left. **(C)** Heatmap depicting the log_2 fold-change over
991 control from iDUX4 expression and HSV-1, HCMV TB40/E, and HCMV AD169r infection in TOs.
992 Genes are ordered by median log_2 fold-change over control. Prioritized genes are marked in gray
993 to the top. **(D-E)** DUX4 and six DSGs were toxic to MRC5 cells. Widefield micrographs of
994 representative fields from HCMV (D) and HSV-1 (E) infection at 24 hpi. Images portray merged
995 TagBFP2 (blue), brightfield (grayscale), and mCherry (D; red; HCMV) or GFP (E; green; HSV-1).
996 **(F)** Schematic of image quantification method. Scale bars = 200 μm.
997

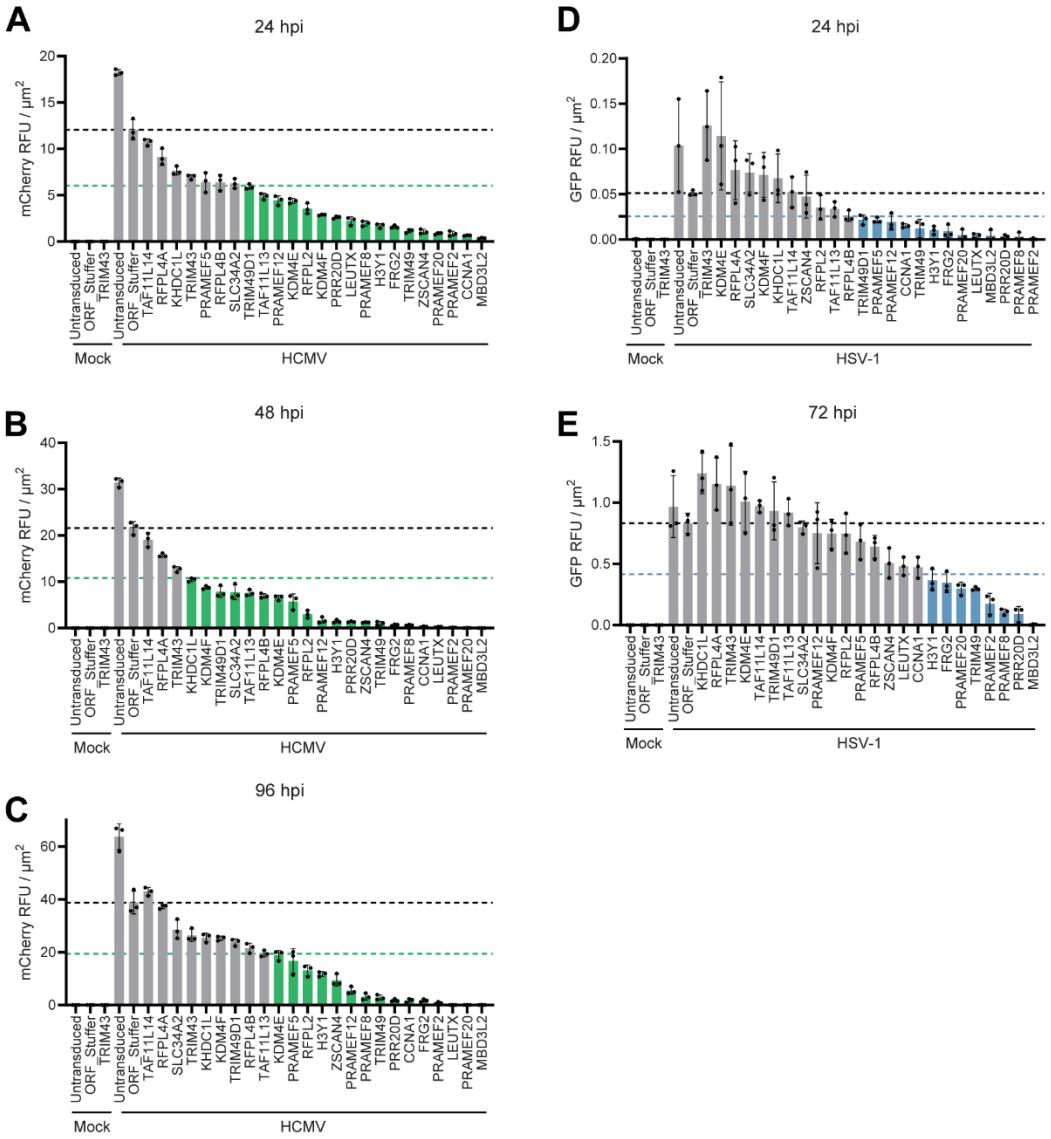

Figure S9 | DUX4-stimulated genes exert anti-herpesvirus activity. (A-C) Bar graphs depicting timepoints for HCMV (A-C) and HSV-1 (D-E) not shown in Figure 6. Black circles represent each individual datapoint. Bars display mean ± SD. Black dashed lines in graphs represent the mean expression of ORF_Stuffer. Colored dashed lines represent 0.5x the black line.

1005 ## References

1006 1. Ander, S.E., Diamond, M.S., and Coyne, C.B. (2019). Immune responses at the maternal-
1007 fetal interface. Sci Immunol *4*. 10.1126/sciimmunol.aat6114.

1008 2. Megli, C.J., and Coyne, C.B. (2022). Infections at the maternal-fetal interface: an overview
1009 of pathogenesis and defence. Nat Rev Microbiol *20*, 67-82. 10.1038/s41579-021-00610-
1010 y.

1011 3. Pontes, K.F.M., Nardozza, L.M.M., Peixoto, A.B., Werner, H., Tonni, G., Granese, R., and
1012 Araujo Junior, E. (2024). Cytomegalovirus and Pregnancy: A Narrative Review. J Clin Med
1013 *13*. 10.3390/jcm13020640.

1014 4. Winter, A.K., and Moss, W.J. (2022). Rubella. Lancet *399*, 1336-1346. 10.1016/S0140-
1015 6736(21)02691-X.

1016 5. Lamont, R.F., Sobel, J.D., Carrington, D., Mazaki-Tovi, S., Kusanovic, J.P., Vaisbuch, E.,
1017 and Romero, R. (2011). Varicella-zoster virus (chickenpox) infection in pregnancy. BJOG
1018 *118*, 1155-1162. 10.1111/j.1471-0528.2011.02983.x.

1019 6. Sandoni, M., Ciardo, L., Tamburini, C., Boncompagni, A., Rossi, C., Guidotti, I., Garetti,
1020 E., Lugli, L., Iughetti, L., and Berardi, A. (2022). Enteroviral Infections in the First Three
1021 Months of Life. Pathogens *11*. 10.3390/pathogens11010060.

1022 7. Shi, T.L., Huang, L.J., Xiong, Y.Q., Zhong, Y.Y., Yang, J.J., Fu, T., Lei, X.F., and Chen,
1023 Q. (2018). The risk of herpes simplex virus and human cytomegalovirus infection during
1024 pregnancy upon adverse pregnancy outcomes: A meta-analysis. J Clin Virol *104*, 48-55.
1025 10.1016/j.jcv.2018.04.016.

1026 8. Delorme-Axford, E., Donker, R.B., Mouillet, J.F., Chu, T., Bayer, A., Ouyang, Y., Wang,
1027 T., Stolz, D.B., Sarkar, S.N., Morelli, A.E., et al. (2013). Human placental trophoblasts
1028 confer viral resistance to recipient cells. Proc Natl Acad Sci U S A *110*, 12048-12053.
1029 10.1073/pnas.1304718110.

1030 9. Bayer, A., Lennemann, N.J., Ouyang, Y., Bramley, J.C., Morosky, S., Marques, E.T., Jr.,
1031 Cherry, S., Sadovsky, Y., and Coyne, C.B. (2016). Type III Interferons Produced by
1032 Human Placental Trophoblasts Confer Protection against Zika Virus Infection. Cell Host
1033 Microbe *19*, 705-712. 10.1016/j.chom.2016.03.008.

1034 10. Pollheimer, J., Vondra, S., Baltayeva, J., Beristain, A.G., and Knofler, M. (2018).
1035 Regulation of Placental Extravillous Trophoblasts by the Maternal Uterine Environment.
1036 Front Immunol *9*, 2597. 10.3389/fimmu.2018.02597.

1037 11. Buchrieser, J., Degrelle, S.A., Couderc, T., Nevers, Q., Disson, O., Manet, C., Donahue,
1038 D.A., Porrot, F., Hillion, K.H., Perthame, E., et al. (2019). IFITM proteins inhibit placental
1039 syncytiotrophoblast formation and promote fetal demise. Science *365*, 176-180.
1040 10.1126/science.aaw7733.

1041 12. Yockey, L.J., Jurado, K.A., Arora, N., Millet, A., Rakib, T., Milano, K.M., Hastings, A.K.,
1042 Fikrig, E., Kong, Y., Horvath, T.L., et al. (2018). Type I interferons instigate fetal demise
1043 after Zika virus infection. Sci Immunol *3*. 10.1126/sciimmunol.aao1680.

1044 13. Zani, A., Zhang, L., McMichael, T.M., Kenney, A.D., Chemudupati, M., Kwiek, J.J., Liu,
1045 S.L., and Yount, J.S. (2019). Interferon-induced transmembrane proteins inhibit cell fusion
1046 mediated by trophoblast syncytins. J Biol Chem *294*, 19844-19851.
1047 10.1074/jbc.AC119.010611.

1048 14. Casazza, R.L., Lazear, H.M., and Miner, J.J. (2020). Protective and Pathogenic Effects of
1049 Interferon Signaling During Pregnancy. Viral Immunol *33*, 3-11. 10.1089/vim.2019.0076.

1050 15. Corry, J., Arora, N., Good, C.A., Sadovsky, Y., and Coyne, C.B. (2017). Organotypic
1051 models of type III interferon-mediated protection from Zika virus infections at the maternal-
1052 fetal interface. Proc Natl Acad Sci U S A *114*, 9433-9438. 10.1073/pnas.1707513114.

1053 16. Wickramage, I., VanWye, J., Max, K., Lockhart, J.H., Hortu, I., Mong, E.F., Canfield, J.,
1054 Lamabadu Warnakulasuriya Patabendige, H.M., Guzeloglu-Kayisli, O., Inoue, K., et al.
1055 (2023). SINE RNA of the imprinted miRNA clusters mediates constitutive type III interferon
1056 expression and antiviral protection in hemochorial placentas. Cell Host Microbe *31*, 1185-
1057 1199 e1110. 10.1016/j.chom.2023.05.018.

1058 17. Yang, L., Semmes, E.C., Ovies, C., Megli, C., Permar, S., Gilner, J.B., and Coyne, C.B.
1059 (2022). Innate immune signaling in trophoblast and decidua organoids defines differential
1060 antiviral defenses at the maternal-fetal interface. Elife *11*. 10.7554/eLife.79794.

1061 18. Rollman, T.B., Berkebile, Z.W., Okae, H., Bardwell, V.J., Gearhart, M.D., and Bierle, C.J.
1062 (2024). Human trophoblast stem cells restrict human cytomegalovirus replication. J Virol
1063 *98*, e0193523. 10.1128/jvi.01935-23.

1064 19. Schatten, H., and Constantinescu, G.M. (2007). Comparative reproductive biology, 1st
1065 Edition (Blackwell Pub.).

1066 20. Wooding, F.B.P., and Burton, G. (2008). Comparative placentation : structures, functions
1067 and evolution (Springer).

1068 21. Berkebile, Z.W., Putri, D.S., Abrahante, J.E., Seelig, D.M., Schleiss, M.R., and Bierle, C.J.
1069 (2021). The Placental Response to Guinea Pig Cytomegalovirus Depends Upon the
1070 Timing of Maternal Infection. Front Immunol *12*, 686415. 10.3389/fimmu.2021.686415.

1071 22. Schleiss, M.R., and McVoy, M.A. (2010). Guinea Pig Cytomegalovirus (GPCMV): A Model
1072 for the Study of the Prevention and Treatment of Maternal-Fetal Transmission. Future Virol
1073 *5*, 207-217. 10.2217/fvl.10.8.

1074 23. Gorman, M.J., Caine, E.A., Zaitsev, K., Begley, M.C., Weger-Lucarelli, J., Uccellini, M.B.,
1075 Tripathi, S., Morrison, J., Yount, B.L., Dinnon, K.H., 3rd, et al. (2018). An
1076 Immunocompetent Mouse Model of Zika Virus Infection. Cell Host Microbe *23*, 672-685
1077 e676. 10.1016/j.chom.2018.04.003.

1078 24. Fisher, S., Genbacev, O., Maidji, E., and Pereira, L. (2000). Human cytomegalovirus
1079 infection of placental cytotrophoblasts in vitro and in utero: implications for transmission
1080 and pathogenesis. J Virol *74*, 6808-6820. 10.1128/jvi.74.15.6808-6820.2000.

1081 25. Weisblum, Y., Panet, A., Zakay-Rones, Z., Vitenshtein, A., Haimov-Kochman, R.,
1082 Goldman-Wohl, D., Oiknine-Djian, E., Yamin, R., Meir, K., Amsalem, H., et al. (2015).

1083 Human cytomegalovirus induces a distinct innate immune response in the maternal-fetal
1084 interface. Virology *485*, 289-296. 10.1016/j.virol.2015.06.023.

1085 26. Schulz, J., Schilling, E., Fabian, C., Zenclussen, A.C., Stojanovska, V., and Claus, C.
1086 (2023). Dissecting Rubella Placental Infection in an In Vitro Trophoblast Model. Int J Mol
1087 Sci *24*. 10.3390/ijms24097894.

1088 27. de la Torre, E., Mulla, M.J., Yu, A.G., Lee, S.J., Kavathas, P.B., and Abrahams, V.M.
1089 (2009). Chlamydia trachomatis infection modulates trophoblast cytokine/chemokine
1090 production. J Immunol *182*, 3735-3745. 10.4049/jimmunol.0800764.

1091 28. Semmes, E.C., and Coyne, C.B. (2022). Innate immune defenses at the maternal-fetal
1092 interface. Curr Opin Immunol *74*, 60-67. 10.1016/j.coi.2021.10.007.

1093 29. Turco, M.Y., Gardner, L., Kay, R.G., Hamilton, R.S., Prater, M., Hollinshead, M.S.,
1094 McWhinnie, A., Esposito, L., Fernando, R., Skelton, H., et al. (2018). Trophoblast
1095 organoids as a model for maternal-fetal interactions during human placentation. Nature
1096 *564*, 263-267. 10.1038/s41586-018-0753-3.

1097 30. Haider, S., Meinhardt, G., Saleh, L., Kunihs, V., Gamperl, M., Kaindl, U., Ellinger, A.,
1098 Burkard, T.R., Fiala, C., Pollheimer, J., et al. (2018). Self-Renewing Trophoblast
1099 Organoids Recapitulate the Developmental Program of the Early Human Placenta. Stem
1100 Cell Reports *11*, 537-551. 10.1016/j.stemcr.2018.07.004.

1101 31. Hendrickson, P.G., Dorais, J.A., Grow, E.J., Whiddon, J.L., Lim, J.W., Wike, C.L., Weaver,
1102 B.D., Pflueger, C., Emery, B.R., Wilcox, A.L., et al. (2017). Conserved roles of mouse DUX
1103 and human DUX4 in activating cleavage-stage genes and MERVL/HERVL
1104 retrotransposons. Nat Genet *49*, 925-934. 10.1038/ng.3844.

1105 32. Bosnakovski, D., Gearhart, M.D., Toso, E.A., Ener, E.T., Choi, S.H., and Kyba, M. (2018).
1106 Low level DUX4 expression disrupts myogenesis through deregulation of myogenic gene
1107 expression. Sci Rep *8*, 16957. 10.1038/s41598-018-35150-8.

1108 33. Rickard, A.M., Petek, L.M., and Miller, D.G. (2015). Endogenous DUX4 expression in
1109 FSHD myotubes is sufficient to cause cell death and disrupts RNA splicing and cell
1110 migration pathways. Hum Mol Genet *24*, 5901-5914. 10.1093/hmg/ddv315.

1111 34. Full, F., van Gent, M., Sparrer, K.M.J., Chiang, C., Zurenski, M.A., Scherer, M.,
1112 Brockmeyer, N.H., Heinzerling, L., Sturzl, M., Korn, K., et al. (2019). Centrosomal protein
1113 TRIM43 restricts herpesvirus infection by regulating nuclear lamina integrity. Nat Microbiol
1114 *4*, 164-176. 10.1038/s41564-018-0285-5.

1115 35. Wyler, E., Franke, V., Menegatti, J., Kocks, C., Boltengagen, A., Praktiknjo, S., Walch-
1116 Ruckheim, B., Bosse, J., Rajewsky, N., Grasser, F., et al. (2019). Single-cell RNA-
1117 sequencing of herpes simplex virus 1-infected cells connects NRF2 activation to an
1118 antiviral program. Nat Commun *10*, 4878. 10.1038/s41467-019-12894-z.

1119 36. Love, M.I., Huber, W., and Anders, S. (2014). Moderated estimation of fold change and
1120 dispersion for RNA-seq data with DESeq2. Genome Biol *15*, 550. 10.1186/s13059-014-
1121 0550-8.

1122 37. Banerji, C.R.S., and Zammit, P.S. (2021). Pathomechanisms and biomarkers in
1123 facioscapulohumeral muscular dystrophy: roles of DUX4 and PAX7. EMBO Mol Med *13*,
1124 e13695. 10.15252/emmm.202013695.

1125 38. Cowley, M.V., Pruller, J., Ganassi, M., Zammit, P.S., and Banerji, C.R.S. (2023). An in
1126 silico FSHD muscle fiber for modeling DUX4 dynamics and predicting the impact of
1127 therapy. Elife *12*. 10.7554/eLife.88345.

1128 39. Arutyunyan, A., Roberts, K., Troule, K., Wong, F.C.K., Sheridan, M.A., Kats, I., Garcia-
1129 Alonso, L., Velten, B., Hoo, R., Ruiz-Morales, E.R., et al. (2023). Spatial multiomics map
1130 of trophoblast development in early pregnancy. Nature *616*, 143-151. 10.1038/s41586-
1131 023-05869-0.

1132 40. Derisoud, E., Jiang, H., Zhao, A., Chavatte-Palmer, P., and Deng, Q. (2024). Revealing
1133 the molecular landscape of human placenta: a systematic review and meta-analysis of
1134 single-cell RNA sequencing studies. Hum Reprod Update *30*, 410-441.
1135 10.1093/humupd/dmae006.

1136 41. Vento-Tormo, R., Efremova, M., Botting, R.A., Turco, M.Y., Vento-Tormo, M., Meyer, K.B.,
1137 Park, J.E., Stephenson, E., Polanski, K., Goncalves, A., et al. (2018). Single-cell
1138 reconstruction of the early maternal-fetal interface in humans. Nature *563*, 347-353.
1139 10.1038/s41586-018-0698-6.

1140 42. Jagannathan, S., Shadle, S.C., Resnick, R., Snider, L., Tawil, R.N., van der Maarel, S.M.,
1141 Bradley, R.K., and Tapscott, S.J. (2016). Model systems of DUX4 expression recapitulate
1142 the transcriptional profile of FSHD cells. Hum Mol Genet *25*, 4419-4431.
1143 10.1093/hmg/ddw271.

1144 43. Wang, D., and Shenk, T. (2005). Human cytomegalovirus UL131 open reading frame is
1145 required for epithelial cell tropism. J Virol *79*, 10330-10338. 10.1128/JVI.79.16.10330-
1146 10338.2005.

1147 44. Street, K., Risso, D., Fletcher, R.B., Das, D., Ngai, J., Yosef, N., Purdom, E., and Dudoit,
1148 S. (2018). Slingshot: cell lineage and pseudotime inference for single-cell transcriptomics.
1149 BMC Genomics *19*, 477. 10.1186/s12864-018-4772-0.

1150 45. Mariot, V., and Dumonceaux, J. (2022). Gene Editing to Tackle Facioscapulohumeral
1151 Muscular Dystrophy. Front Genome Ed *4*, 937879. 10.3389/fgeed.2022.937879.

1152 46. Winokur, S.T., Bengtsson, U., Vargas, J.C., Wasmuth, J.J., Altherr, M.R., Weiffenbach, B.,
1153 and Jacobsen, S.J. (1996). The evolutionary distribution and structural organization of the
1154 homeobox-containing repeat D4Z4 indicates a functional role for the ancestral copy in the
1155 FSHD region. Hum Mol Genet *5*, 1567-1575. 10.1093/hmg/5.10.1567.

1156 47. Himeda, C.L., Jones, T.I., and Jones, P.L. (2016). CRISPR/dCas9-mediated
1157 Transcriptional Inhibition Ameliorates the Epigenetic Dysregulation at D4Z4 and
1158 Represses DUX4-fl in FSH Muscular Dystrophy. Mol Ther *24*, 527-535.
1159 10.1038/mt.2015.200.

1160 48. Sikrova, D., Cadar, V.A., Ariyurek, Y., Laros, J.F.J., Balog, J., and van der Maarel, S.M.
1161 (2021). Adenine base editing of the DUX4 polyadenylation signal for targeted genetic

1162 therapy in facioscapulohumeral muscular dystrophy. Mol Ther Nucleic Acids *25*, 342-354.
1163 10.1016/j.omtn.2021.05.020.

1164 49. Mitsuhashi, H., Ishimaru, S., Homma, S., Yu, B., Honma, Y., Beermann, M.L., and Miller,
1165 J.B. (2018). Functional domains of the FSHD-associated DUX4 protein. Biol Open *7*.
1166 10.1242/bio.033977.

1167 50. Friedel, C.C., Whisnant, A.W., Djakovic, L., Rutkowski, A.J., Friedl, M.S., Kluge, M.,
1168 Williamson, J.C., Sai, S., Vidal, R.O., Sauer, S., et al. (2021). Dissecting Herpes Simplex
1169 Virus 1-Induced Host Shutoff at the RNA Level. J Virol *95*. 10.1128/JVI.01399-20.

1170 51. Full, F., Walter, S., Neugebauer, E., Tan, J., Drayman, N., Franke, V., Tay, S., Landthaler,
1171 M., Akalin, A., Ensser, A., and Wyler, E. (2023). Herpesviruses mimic zygotic genome
1172 activation to promote viral replication. Res Sq. 10.21203/rs.3.rs-3125635/v1.

1173 52. Tan, J., Franke, V., Neugebauer, E., Lagisquet, J., Kuderna, A.K., Walter, S., Ensser, A.,
1174 Landthaler, M., Stamminger, T., Gramberg, T., et al. (2024). DNA virus infections shape
1175 transposable elements activity in vitro and in vivo. Biorxiv.

1176 53. Liu, D., Matzuk, M.M., Sung, W.K., Guo, Q., Wang, P., and Wolgemuth, D.J. (1998). Cyclin
1177 A1 is required for meiosis in the male mouse. Nature Genetics *20*, 377-380. 10.1038/3855.

1178 54. Oduro, J.D., Uecker, R., Hagemeier, C., and Wiebusch, L. (2012). Inhibition of human
1179 cytomegalovirus immediate-early gene expression by cyclin A2-dependent kinase activity.
1180 J Virol *86*, 9369-9383. 10.1128/JVI.07181-11.

1181 55. Epping, M.T., Wang, L., Edel, M.J., Carlee, L., Hernandez, M., and Bernards, R. (2005).
1182 The human tumor antigen PRAME is a dominant repressor of retinoic acid receptor
1183 signaling. Cell *122*, 835-847. 10.1016/j.cell.2005.07.003.

1184 56. Kern, C.H., Yang, M., and Liu, W.S. (2021). The PRAME family of cancer testis antigens
1185 is essential for germline development and gametogenesisdagger. Biol Reprod *105*, 290-
1186 304. 10.1093/biolre/ioab074.

1187 57. Birtle, Z., Goodstadt, L., and Ponting, C. (2005). Duplication and positive selection among
1188 hominin-specific PRAME genes. BMC Genomics *6*, 120. 10.1186/1471-2164-6-120.

1189 58. Katayama, S., Ranga, V., Jouhilahti, E.M., Airenne, T.T., Johnson, M.S., Mukherjee, K.,
1190 Burglin, T.R., and Kere, J. (2018). Phylogenetic and mutational analyses of human LEUTX,
1191 a homeobox gene implicated in embryogenesis. Sci Rep *8*, 17421. 10.1038/s41598-018-
1192 35547-5.

1193 59. Lewin, T.D., Blagrove, J.R., and Holland, P.W.H. (2023). Rapid Evolution of the
1194 Embryonically Expressed Homeobox Gene LEUTX within Primates. Genome Biol Evol *15*.
1195 10.1093/gbe/evad097.

1196 60. Thaxton, J.E., Nevers, T., Lippe, E.O., Blois, S.M., Saito, S., and Sharma, S. (2013).
1197 NKG2D blockade inhibits poly(I:C)-triggered fetal loss in wild type but not in IL-10-/- mice.
1198 J Immunol *190*, 3639-3647. 10.4049/jimmunol.1203488.

1199 61. Thwaites, D.T., and Anderson, C.M. (2011). The SLC36 family of proton-coupled amino
1200 acid transporters and their potential role in drug transport. Br J Pharmacol *164*, 1802-1816.
1201 10.1111/j.1476-5381.2011.01438.x.

1202 62. Marks, J. (2019). The role of SLC34A2 in intestinal phosphate absorption and phosphate
1203 homeostasis. Pflugers Arch *471*, 165-173. 10.1007/s00424-018-2221-1.

1204 63. Yang, L., Liang, P., Yang, H., and Coyne, C.B. (2024). Trophoblast organoids with
1205 physiological polarity model placental structure and function. J Cell Sci *137*.
1206 10.1242/jcs.261528.

1207 64. Turco, M.Y., Gardner, L., Hughes, J., Cindrova-Davies, T., Gomez, M.J., Farrell, L.,
1208 Hollinshead, M., Marsh, S.G.E., Brosens, J.J., Critchley, H.O., et al. (2017). Long-term,
1209 hormone-responsive organoid cultures of human endometrium in a chemically defined
1210 medium. Nat Cell Biol *19*, 568-577. 10.1038/ncb3516.

1211 65. O'Connor, C.M., and Shenk, T. (2011). Human cytomegalovirus pUS27 G protein-coupled
1212 receptor homologue is required for efficient spread by the extracellular route but not for
1213 direct cell-to-cell spread. J Virol *85*, 3700-3707. 10.1128/JVI.02442-10.

1214 66. Cockrell, S.K., Sanchez, M.E., Erazo, A., and Homa, F.L. (2009). Role of the UL25 protein
1215 in herpes simplex virus DNA encapsidation. J Virol *83*, 47-57. 10.1128/JVI.01889-08.

1216 67. Bayer, A., Delorme-Axford, E., Sleigher, C., Frey, T.K., Trobaugh, D.W., Klimstra, W.B.,
1217 Emert-Sedlak, L.A., Smithgall, T.E., Kinchington, P.R., Vadia, S., et al. (2015). Human
1218 trophoblasts confer resistance to viruses implicated in perinatal infection. Am J Obstet
1219 Gynecol *212*, 71 e71-71 e78. 10.1016/j.ajog.2014.07.060.

1220 68. Wells, A.I., Grimes, K.A., and Coyne, C.B. (2022). Enterovirus Replication and
1221 Dissemination Are Differentially Controlled by Type I and III Interferons in the
1222 Gastrointestinal Tract. mBio *13*, e0044322. 10.1128/mbio.00443-22.

1223 69. Johnson, W.E., Li, C., and Rabinovic, A. (2007). Adjusting batch effects in microarray
1224 expression data using empirical Bayes methods. Biostatistics *8*, 118-127.
1225 10.1093/biostatistics/kxj037.

1226 70. Hao, Y., Hao, S., Andersen-Nissen, E., Mauck, W.M., 3rd, Zheng, S., Butler, A., Lee, M.J.,
1227 Wilk, A.J., Darby, C., Zager, M., et al. (2021). Integrated analysis of multimodal single-cell
1228 data. Cell *184*, 3573-3587 e3529. 10.1016/j.cell.2021.04.048.

1229 71. Linderman, G.C., Zhao, J., Roulis, M., Bielecki, P., Flavell, R.A., Nadler, B., and Kluger,
1230 Y. (2022). Zero-preserving imputation of single-cell RNA-seq data. Nat Commun *13*, 192.
1231 10.1038/s41467-021-27729-z.

1232 72. Korsunsky, I., Millard, N., Fan, J., Slowikowski, K., Zhang, F., Wei, K., Baglaenko, Y.,
1233 Brenner, M., Loh, P.R., and Raychaudhuri, S. (2019). Fast, sensitive and accurate
1234 integration of single-cell data with Harmony. Nat Methods *16*, 1289-1296.
1235 10.1038/s41592-019-0619-0.

1236 73. Zappia, L., and Oshlack, A. (2018). Clustering trees: a visualization for evaluating
1237 clusterings at multiple resolutions. Gigascience *7*. 10.1093/gigascience/giy083.

1238 74. Dremel, S.E., and DeLuca, N.A. (2019). Genome replication affects transcription factor
1239 binding mediating the cascade of herpes simplex virus transcription. Proc Natl Acad Sci
1240 U S A *116*, 3734-3739. 10.1073/pnas.1818463116.

1241 75. Van den Berge, K., Roux de Bezieux, H., Street, K., Saelens, W., Cannoodt, R., Saeys,
1242 Y., Dudoit, S., and Clement, L. (2020). Trajectory-based differential expression analysis
1243 for single-cell sequencing data. Nat Commun *11*, 1201. 10.1038/s41467-020-14766-3.
1244